FLORIAN GOTH

A QUANTUM MONTE-CARLO METHOD FOR SYSTEMS OUT OF EQUILIBRIUM

A QUANTUM MONTE-CARLO METHOD FOR SYSTEMS OUT OF EQUILIBRIUM

FLORIAN GOTH

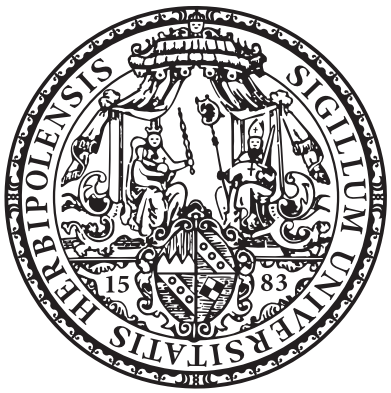

Theoretische Physik 1
Institut für theoretische Physik und Astrophysik
Julius-Maximilians-Universität Würzburg

September 2009

SUPERVISORS:
Prof. Dr. Fakher F. Assaad

ABSTRACT

In this thesis we investigate an extension of the Diagrammatic Determinantal Quantum Monte-Carlo method to real times. To that end we employed a Keldysh-formalism which allows us to jointly construct a perturbation theory in imaginary and real time. This enables us to study the time dependent evolution of a thermal initial state. The feasibility and the limits of the method arising due to the dynamical sign problem are discussed with respect to simple toy-models. As a notable application we study an experiment from the field of ultracold atoms in optical lattices. We examine the reaction of a correlated electron system to the sudden change of one of its parameters.

ZUSAMMENFASSUNG

In der vorliegenden Arbeit beschäftigten wir uns mit einer Erweiterung des Diagrammatischen Quanten-Monte-Carlo auf reale Zeiten. Hierzu wurde ein Keldysh-Formalismus benutzt, der die Möglichkeit bietet eine Störungstheorie gleichwertig in imaginärer und realer Zeit zu entwickeln. Mit dieser Methode ist es möglich die zeitliche Evolution korrelierter thermischer Zustände durchzuführen. Die Implementierbarkeit und die Grenzen dieses Verfahrens aufgrund des dynamischen Vorzeichenproblems werden anhand einfacher Spielzeug-Modelle diskutiert. Als besondere Anwendung wird ein Experiment aus dem Bereich ultrakalter Atome in optischen Gittern betrachtet, bei dem untersucht wird wie ein korreliertes Elektronen-System auf die plötzliche Änderung eines Umgebungsparameters reagiert.

CONTENTS

LIST OF FIGURES

ACRONYMS

QMC Quantum Monte Carlo

DDQMC Diagrammatic Determinantal QMC

DMFT Dynamical Mean Field Theory

HTSC High Temperature Super Conductivity

fRG functional Renormalization Group

ED Exact Diagonalization

ETH Eigenstate Thermalization Hypothesis

NEGF Non-equilibrium Green's function

DMRG Density-Matrix Renormalization Group

1 INTRODUCTION

"Good morning," said the little prince.
"Good morning," said the merchant.
This was a merchant who sold pills
that had been invented to quench thirst.
You need only swallow one pill a week,
and you would feel no need of anything to drink.
"Why are you selling those?" asked the little prince.
"Because they save a tremendous amount of time," said the merchant.
"Computations have been made by experts. With these pills,
you save fifty-three minutes in every week."
"And what do I do with those fifty-three minutes?"
"Anything you like..."
"As for me," said the little prince to himself,
"if I had fifty-three minutes to spend as I liked,
I should walk at my leisure toward a spring of fresh water..."

— *Antoine de Saint-Exupéry* [1]

For ages humans have philosophized about the meaning of time, its role for their lives and what to do with the time in between. Thus one wonders that the study of correlated electrons got by mostly without including explicit realtime-dependencies into their model systems. If we neglect the correlations and assume the picture of nearly independent electrons we can, with some success, get by with (numerically) solving the Schrödinger equation. But a lot of the more interesting effects like superconductivity in high-T_C superconductors can only be understood if we include the strong correlations present in the host materials which are due to the strong Coulomb repulsion in those compounds. These correlation induced effects pose serious challenges for themselves, thus a lot of work during the past decades focused on the study of a material's equilibrium properties. Concurrently, this period saw the rising use of computers in home use as well as in the scientific community and thus we now have a solid amount of methods that allow for the study of equilibrium properties while taking advantage of the computational power that today's sophisticated computers offer. The main tools at hand today are Exact Diagonalization (ED), Density-Matrix Renormalization Group (DMRG) methods and, of course, Quantum Monte Carlo (QMC) methods. These numerical tools offer the possibility to verify analytical results gained by e.g. perturbation theory and offer an unbiased approach to physics in general and especially allow the study of intermediate regimes of a models parameters where analytical methods are almost never applicable. QMC offers a lot of flexibility to design algorithms for a concrete problem, is easily parallizable and the computational cost often only scales like a power law, if the dreaded sign problem is absent. The obtained results are exact within their statistical error bars. This was all well and nice for thermodynamics but to get back at the quote, how did time-dependency enter solid-state

physics? Already in the Matsubara-formalism it was possible to derive the response of a system in linear response theory, if the external perturbation is small, via the Kubo-formula [2]. But if one was interested in results beyond linear response it was necessary to develop other means. Already some 50 years ago Schwinger [3] and Keldysh[4] worked on the problem of constructing perturbation theories that allowed the calculation of time-dependent correlation functions. Of particular importance is Schwinger's introduction of the closed time-path Green's function. Their theory allowed for the calculation of time-dependent correlation functions but assumed that the initial state is not a correlated state. Thus one was looking for theories that allowed the initial state to be a correlated one. Fujita made the first progress to include the initial correlations [5, 6] via influence functions and discussed the decay of these initial correlations. Later, Hall [7] simplified the theory by introducing Green's functions and derived a Wick's theorem that includes the initial correlations. After that, a complete overview over Non-equilibrium Green's function (NEGF) techniques up to that point in time was given by Danielewicz[8]. He clarified the Green's function formalism, derived a Wick's theorem (and the conditions of its validity) and studied the conditions for the validity of the Boltzmann equation. In the 90s, Wagner [9] showed that the density matrix for the averaging process need not be a thermal density-matrix and recast the perturbative expansion of the Green's function into one where the Green's function has a 3x3-matrix structure and showed how Matsubara, Feynman and Keldysh theory can be recovered as special cases of the theory. At the end of that decade there was a renewed interest into functional integral methods that are derived within the Contourpath framework [10, 11, 12].

Or one assumes that the many-particle interactions are switched on adiabatically

As at the beginning of this century a lot of numerical methods for tackling thermodynamic properties were available there was an increased interest in reformulating those ideas in a way that allowed the investigation of time-dependent problems beyond the limits of linear response theory. Examples are the application of a Keldysh-formalism to Density Functional Theory in [13, 14] to study time-dependent properties or the formulation of a time-dependent version of Dynamical Mean Field Theory (DMFT) in [15, 16]. In the context of this diploma thesis we may of course not forget recent formulations of QMC methods on the realtime Keldysh-contour [17, 18]. It is an interesting note, that the inclusion of correlated initial states is not only of interest to solid-state physicists but to people from high energy physics as well [19]. Here we also find attempts to include the imaginary part of the extended contour (clarified in Figure 3) into the realtime part of the contour [20]. Also from the field of high energy physics stems the only alternative (known to the author) to the Keldysh-formalism: Umezawas Thermofield Dynamics approach [22, 19, 23, 24, 25] whose use seems to have spread not that far from effects in HEP [26].

see [21] for the instructive case of the harmonic oscillator in TFD.

That concludes this review of the historical development of realtime theories, so let's take a look at the problems people have studied using Keldysh-methods. In solid-state physics Keldysh-methods were used to study non-equilibrium super-conductivity and quantum effects in disordered systems[27, 28]. Already Keldysh used his technique [4] to derive kinetic equations for the equilibrium properties of interacting electrons with phonons. The Keldysh-method found use in transport theory because of the greater generality it allowed. As arbitrary interac-

tions can be inserted into the formalism it is possible to study nonlinear effects that are not in reach of linear response theory. A traditional example is the transport theory of metals (see the overview in [28]). The transport through a metallic junction given a time-dependent external potential at the electrodes is discussed in [29] and an expression for the current is derived. The author claims [30] that this represents an extension of the established Landauer formalism. The transport through an interacting electron system given a static potential bias between the leads was derived in [31]. These impurity models gained a lot of interest recently as they are the mathematical models of quantum dots that are coupled to some metallic leads. In contrast to their equilibrium properties, about their non-equilibrium behaviour is much less known. The origins of the non-equilibrium situation can be quite different. The most obvious one would be an external interaction that is switched on at some time. A system can also be placed out of equilibrium by starting from an atypical initial condition or it can be placed between infinite external reservoirs that impose the out-of equilibrium situation.

The widespread use of QMC methods starts with the invention of algorithms that are applicable to impurity models. The method of choice was the Hirsch-Fye algorithm, invented in 1986 [32]. Employing the Trotter-decomposition at finite imaginary time slices, the Hirsch-Fye algorithm suffers from a systematic discretization error. This problem was overcome by the development of the Diagrammatic Determinantal QMC (DDQMC) algorithm in 2005 [33] which is not employing any discretization scheme and as such is accurate up to machine precision within its error bars. We employ the DDQMC method where we expand in powers of the interaction, nevertheless there exist variants that expand in the hybridization to the leads [34]. The method is directly derived from a path integral formulation of the partition function Z, thus it provides a great deal of flexibility. The partition function is then expanded into its diagrams and the resulting diagrams get summed up via the stochastic process. For a given perturbation order a set of interaction vertices is generated whose corresponding Feynman diagrams get summed up by invoking Wick's theorem. As the method has its roots in a formulation of the partition function in the action the method is easily extended to include not only the imaginary time τ but also the Keldysh-Contour. Having done that, the method is ready for dealing with situations out of equilibrium. Similar work along the same lines was reported in [18, 17].

Because of this property it is a Continuous Time QMC (CTQMC) method. This sets it apart from Hirsch-Fye because of its lacking systematic error.

As an application outside of the toy-model regime we investigate the time-dependent response of a one-dimensional Hubbard-chain to the removal of the interaction term H_U. This contrasts with studies done in [35] where the quench of free electrons to the sudden switch on of H_U was studied. Using DMFT with a QMC impurity solver they lack access to spatially resolved correlation functions. Experimentally these quench dynamics are realized using experiments with ultracold atoms [36]. The atoms get trapped with electromagnetic fields in the ultra high vacuum and additional external magnetic fields can be used to tune the interaction strength of the atoms from attractive to repulsive. Being trapped in the vacuum their isolation from the rest of the world is close to perfect. By tuning the interaction to the right regime it is possible to create highly correlated electron systems which are characterized by the competition between the kinetic energy and the interactions. The ensemble of atoms gets structured using laser induced potentials,

This allows a realization of a theoretical model that will propably never be achieved in a solid-state experiment.

that way the lattice structure forms. The dimensionality gets controlled by the confinement of the optical potential that restricts the electron movement to low dimensions. In the study of these low-dimensional systems the most pressing questions are

- Does the system evolve to a new steady state?
- Under what circumstances does the system evolve to a new steady state?
- If it does, what is the nature of this state?
- Does the system retain memory of the initial state?

In those cases that lead to a new thermal state a natural question is, how the interplay between the unitarity of the time-evolution of quantum mechanics and the vast amount of degrees of freedom in a many-body sytem lead to the observed long-time behaviour. This question is addressed by the Eigenstate Thermalization Hypothesis (ETH) in Chapter 6.

Part I

THE THEORY

2 PERTURBATION THEORY 101

I was born not knowing and have had
only a little time to change that here and there.

— Richard Feynman

This chapter introduces the basic theory from which we will later derive a QMC method suitable for the implementation on a computer. We start by introducing some venerable attempts at constructing perturbation theories for dealing with time-dependent problems in a canonical formulation, will analyze their deficiencies and improve on them. Having constructed a theory that fits our needs we will cast it in a form of functional integrals and proceed to the derivation of a QMC algorithm.

Here we assume the usual decomposition of the Hamilton-operator in a solvable problem given by H_0 and a possibly time-dependent interaction V. The full problem is then given by

$$H = H_0 + V. \tag{2.1}$$

For connections to the other pictures, see the literature ([37, 30, 2])

Next we state some known results about time-evolution in the Dirac-picture. Dirac's time-evolution-operator U fulfills the known differential equation

$$i\frac{d}{dt}U(t,t') = V(t)U(t,t') \tag{2.2}$$

whose solution can be written in the form of a time-ordered exponential

$$\begin{aligned} U(t,t') &= T\exp(-i\int_{t'}^{t} dt''V(t'')) \\ &= \sum_{n=0}^{\infty} \frac{(-i)^n}{n!} T^C \int_{t_0}^{t} dt_1 .... \int_{t_0}^{t} dt_n V(t_1)...V(t_n) \end{aligned} \tag{2.3}$$

with the time-ordering T^C on a linear piece of time of the real axis. The connection to the Schrödinger-picture is

$$U(t,t') = U_0^{-1}(t,t_0)U_S(t,t')U_0(t',t_0) \tag{2.4}$$

with $U_0^{-1}(t',t) = e^{-iH_0(t-t')}$ and U_S is the time-evolution in the Schrödinger-picture.

2.1 FEYNMAN'S PERTURBATION THEORY

Let's start out with the possibly familiar perturbation theory by Feynman [37]. We begin by examining an expectation value in the Heisenberg-picture

$$O(t) = \langle 0|O_H(t)|0\rangle \tag{2.5}$$

Thus at $t = -\infty$ the system is in the non-interacting state $|-\infty\rangle$.

where $|0\rangle$ is the ground state of the full interacting Hamiltonian. But we don't know the interacting ground-state $|0\rangle$, so we need to express it in terms of the normalized non-interacting ground-state $|-\infty\rangle$. To achieve some progress towards this goal we just have to make the first assumption: that the Hamiltonian has no time-dependency. Then we can artificially introduce the adiabatic switching on of the interaction:

Here α is a positive infinitesimal $\alpha = 0^+$.

$$V(t) = Ve^{-\alpha|t|}.$$

Note, that the interaction is symmetrically switched on in the past as it is switched off in the future. For these adiabatic types of switching procedures the Gell-Mann-Low theorem provides the connection between the fully interacting and the non-interacting state,

$$|0\rangle = U(0,-\infty)|-\infty\rangle \tag{2.6}$$

with the time-evolution-operator $U(t,t')$ of the interaction-picture. We also transform the observable O_H to the interaction-picture according to

$$A_H(t) = U(0,t)A_I(t)U(t,0). \tag{2.7}$$

We get for the expectation-value

$$O(t) = \langle -\infty|U(-\infty,0)U(0,t)O_I(t)U(t,0)U(0,-\infty)|-\infty\rangle. \tag{2.8}$$

This Ordering *will get clearer later on.*

To achieve some kind of ordering of the operators we start to rewrite the left-hand bra-vector:

$$\langle -\infty|U(-\infty,0) = \langle\infty|U(\infty,-\infty)U(-\infty,0). \tag{2.9}$$

That brings eq. (2.8) to:

$$\begin{aligned} O(t) &= \langle\infty|U(\infty,-\infty)U(-\infty,0)U(0,t)O_I(t)U(t,0)U(0,-\infty)|-\infty\rangle \\ &= \langle\infty|U(\infty,-\infty)U(-\infty,t)O_I(t)U(t,-\infty)|-\infty\rangle. \end{aligned} \tag{2.10}$$

We can connect that state in the future with the state in the past if we make the additional assumption, that the non-interacting ground-state is non-degenerate. Then, because of the symmetry in time of the switching procedure, they should be equal up to a phase-factor e^{iL}:

$$|\infty\rangle = e^{iL}|-\infty\rangle. \tag{2.11}$$

We determine this phase-factor as follows:

$$\begin{aligned} |\infty\rangle &= U(\infty,0)|0\rangle \\ &= U(\infty,0)U(0,-\infty)|-\infty\rangle \\ &= U(\infty,-\infty)|-\infty\rangle \\ &\overset{!(2.11)}{=} e^{iL}|-\infty\rangle. \end{aligned} \tag{2.12}$$

Now, multiplying the last two lines with $\langle-\infty|$ from the left, we get the relation for e^{iL}:

$$e^{iL} = \langle -\infty|U(\infty,-\infty)|-\infty\rangle. \tag{2.13}$$

Inserting this into eq. (2.10) we are almost done as the final expression doesn't contain any references to states in the future anymore:

$$\begin{aligned} O(t) &= \langle\infty|U(\infty,t)O_I(t)U(t,-\infty)|-\infty\rangle \\ &= e^{-iL}\langle-\infty|\underbrace{U(\infty,t)}_{\in[t,\infty]}O_I(t)\underbrace{U(t,-\infty)}_{\in[-\infty,t]}|-\infty\rangle. \end{aligned} \tag{2.14}$$

Note that the time-evolution-operators are already in a time-ordered order, thus we can insert a time-ordering-operator T,

$$\begin{aligned} O(t) &= e^{-iL}\langle-\infty|TU(\infty,t)O_I(t)U(t,-\infty)|-\infty\rangle \\ &= \frac{\langle-\infty|TU(\infty,-\infty)O_I(t)|-\infty\rangle}{\langle-\infty|U(\infty,-\infty)|-\infty\rangle}. \end{aligned} \tag{2.15}$$

As the T-operator sorted all operators to their respective places, we were able to join the time-evolution-operators and therefore arrived at the final expression of Feynman-perturbation-theory. Now one can start expanding $U(\infty,-\infty)$ and calculate observables to any desired order, provided the initial non-interacting ground-state allows a Wick-decomposition. This expansion can be cast into diagrams and as usual the vacuum amplitude(the denominator of eq. (2.15)) cancels.

This is actually not a new assumption , as this ground-state should allow a Wick-decomposition provided it was really non-interacting.

In the course of getting till here we collected quite a bunch of assumptions:

- H may contain interactions but no time-dependency, else we can't employ Gell-Mann-Low's-Theorem(2.6).
- The non-interacting ground-state $|-\infty\rangle$ must be non-degenerate.
- $|-\infty\rangle$ must allow a Wick-decomposition.

So let's see if we can do better with Keldysh's theory.

2.2 KELDYSH'S THEORY

Again, we're interested in the expectation value of an operator O at time t starting from an initial time t_0, but this time we want to allow for explicitly time-dependent Hamiltonians $H = H(t)$. We can still do this by evolving some initial state $|\rangle$ given at a time t_0 to the time t, let the operator act and evolve back:

$$O(t) = \langle|O_H(t)|\rangle = \langle|U(t_0,t)O_I(t)U(t,t_0)|\rangle. \tag{2.16}$$

From here on everything is in the interaction picture.

We proceed to cast those two time-evolution-operators in the form of time-ordered exponentials [8]. The left one is

$$U(t_0,t) = \sum_{n=0}^{\infty}\frac{(-i)^n}{n!}T^A\int_t^{t_0}dt_1....\int_t^{t_0}dt_n V(t_1)...V(t_n) \tag{2.17}$$

and the right one is

$$U(t,t_0) = \sum_{n=0}^{\infty}\frac{(-i)^n}{n!}T^C\int_{t_0}^{t}dt_1....\int_{t_0}^{t}dt_n V(t_1)...V(t_n). \tag{2.18}$$

They're conjugate to each other, so what do you do if you take the complex conjugate of (2.18)? you put a minus before the i (compensated by interchanging the limits of integration), then reverse the order of the operators (compensated by T^A).

Here we introduced two new time-ordering operators, the chronological one, T^C, with

$$T^C(A(t_1)B(t_2)) = \Theta(t_1-t_2)A(t_1)B(t_2) - \Theta(t_2-t_1)B(t_2)A(t_1),$$

which sorts the greatest time to the left and the anti-chronological one, T^A, with

$$T^A(A(t_1)B(t_2)) = \Theta(t_2 - t_1)A(t_1)B(t_2) - \Theta(t_1 - t_2)B(t_2)A(t_1),$$

which sorts the greatest time to the right. Introducing the time-ordered exponentials into eq. (2.16) we get

$$O(t) = \langle T^A \exp(-i \int_{t}^{t_0} dt' V_I(t')) O_I(t) T^C \exp(-i \int_{t_0}^{t} dt' V_I(t')) \rangle. \quad (2.19)$$

We could construct a theory with the same diagrammatic expansion as the previous Feynman-theory, if we were able to join those two exponentials. To achieve that we introduce a new time-ordering operator T_{C_K} that recognizes whether an operator belongs on the left side (T^A is acting here) of the observable or on the right (this is where T^C acts). Additionally, as an mnemonic to remember the ordering, we introduce the famous Keldysh-contour.

This theory thus gets around referencing a state in the far future, by taking instead the initial state again.

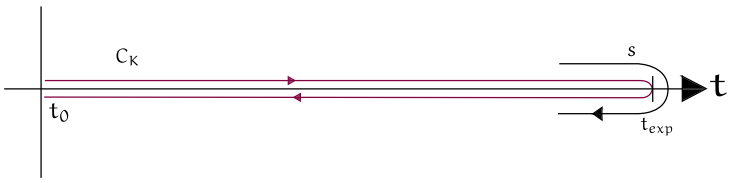

Figure 1: This is the Keldysh-contour C_K starting at some initial time t_0 and extending up to the maximum expansion time t_{exp}. On the x-axis is the real-time. Along the whole contour lives the contour-time-variable s.

The definition of T_{C_K} is thus

$$T_{C_K} A(s)B(s') = A(s)B(s')\Theta(s - s') - B(s')A(s)\Theta(s' - s) \quad (2.20)$$

where s is now a value along the Keldysh-contour, therefore it is from the interval $[0, 2t_{exp}]$. If we take a look at a bunch of operators, there are four possibilities, two where s and s' reside on the same part of the contour:

Note the ordering that is still operating on these parts of the contour.

$$T_{C_K}(A(s)B(s')) = T^C(A(t)B(t')) \text{ s,s' are on the forward branch,}$$
$$T_{C_K}(A(s)B(s')) = T^A(A(t)B(t')) \text{ s,s' are on the backward branch.}$$

s, s' are on different parts of the contour, thus we know which order the operators are in and can evaluate the T-operators.

and two where they are on different parts:

$$T_{C_K}(A(s)B(s')) = -B(t')A(t) \text{ s is on the forward,}$$
$$T_{C_K}(A(s)B(s')) = A(t)B(t') \text{ s' is on the forward.}$$

As s and s' still point to real times we were able to replace the contour times by their linear equivalents on the real axis.

T_{C_K} is now able to sort the chronological and antichronolgical parts on their corresponding sides, so we can rewrite eq. (2.19) as

$$O(s) = \langle T_{C_K} \exp(-i \int_{C_K} dz' V(z')) O_I(s) \rangle = \langle T_{C_K} S_{C_K} O_I(s) \rangle. \quad (2.21)$$

We have allowed to evaluate the observable at contour-times s, thus you expect $O(s)$ with s taken on the forward branch, to be the same as if s is taken on the backward branch, because the two branches have to be physically indistinguishable. So far, the length of the Keldysh-contour seems to be given by the time of the observable that one is interested in, but if we look at eq. (2.19) we see, that we can insert additional time-evolution-operators symmetrically on both sides of the observable and in that way elongate the contour up to infinity. You just have to make sure that you have all points in time you are interested in included. We didn't say anything about the initial state with which we take the average, but it is clear, that if the Keldysh theory is to be useful, it must be a state that allows a Wick-decomposition. Then we can expand the exponential in eq. (2.21) and construct a perturbation theory as usual.

Useful for debugging!

Time-evolution still fulfills the group-property.

So on what parts of Feynman's theory did we improve?

- An explicit time-dependence is allowed.
- We don't need to invoke Gell-Mann-Low's theorem(eq. (2.6)), as we don't need any assumptions about an adiabatic switching procedure.
- No information about the final state needed.

But still, we need to assume that the state used for averaging allows a Wick-decomposition. In certain applications (e.g. particle physics) this is a valid assumption, as the initial state is one of a free particle, but in solid-state physics we often like to treat correlated initial states that we can't cover in Keldysh's theory; or only if we assume that we are looking at times where those initial correlations aren't dominant.

So this requires systems where they can actually decay.

2.3 WHAT ABOUT CORRELATED INITIAL STATES?

2.3.1 *Imaginary-Time-Formalism*

Let's start by recapitulating some pieces of the imaginary-time formalism [9]. The thermal average of an observable is given by

Here $H = H_0 + V$ and time - independent.

$$O = \mathrm{Tr}(\rho O) \tag{2.22}$$

with a given density-matrix ρ. Actually it can be arbitrary(see [9]), but we restrict ourselves to the thermal case where

$$\rho = \frac{e^{-\beta H}}{Z}$$

with the partition function $Z = \mathrm{Tr} e^{-\beta H}$. We also define a density-matrix for the non-interacting system H_0 ,

$$\rho_0 = \frac{e^{-\beta H_0}}{Z_0}$$

with $Z_0 = \mathrm{Tr} e^{-\beta H_0}$. With that we can rewrite the density-matrix of the interacting system as:

$$\begin{aligned} \rho &= \frac{1}{Z} e^{-\beta H_0} e^{\beta H_0} e^{-\beta H} \\ &= \frac{Z_0}{Z} \rho_0 e^{\beta H_0} e^{-\beta H} \end{aligned} \tag{2.23}$$

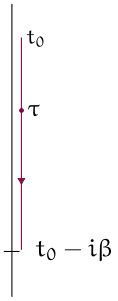

Figure 2: The contour to visualize the ordering on the imaginary axis.

which is, employing eq. (2.4),

$$\rho = \frac{Z_0}{Z}\rho_0 U(-i\beta, 0). \tag{2.24}$$

τ is used to distinguish the time from true real times.

In the last line we used the interaction-picture time-evolution $U(\tau, \tau')$ and allowed its evaluation for complex times. $U(\tau, \tau')$ can also be written in the form of a time-ordered exponential(see eq. (2.3)), with the distinction that T sorts along the imaginary axis in $[0, -i\beta]$, which corresponds to an ordering along the contour of Figure 2.

With this expression(eq. (2.24)) we can rewrite the thermal average,

$$\langle O\rangle = \mathrm{Tr}(\rho O) = \frac{Z_0}{Z}\mathrm{Tr}(\rho_0 U_D(-i\beta, 0)O\rangle \tag{2.25}$$

and now one can envision the perturbative expansion in a similar way as before.

2.3.2 *Piecing it all together*

Now, having separate expansions for the density-matrix and the time-evolution we can start piecing the parts of the puzzle together [9]. Let's take a look at the thermal average of a time-dependent observable,

$$O(t) = \mathrm{Tr}(\rho O_H(t)). \tag{2.26}$$

We insert the expansions of the initial density matrix(see eq. (2.25)) and of the time-evolution of $O_H(t)$(see eq. (2.21)), which leads us to

$$O(s) = \mathrm{Tr}(\rho_0 U(-i\beta, 0)\mathcal{T}_{C_K}[S_{C_K}O(s)]).$$

We now employ the same trick as in the section before and introduce a new contour and a new common time-ordering. To that end we introduce our final contour C (see Figure 3) Then we can join the expansions of the real-time-evolution-operator S_{C_K} and of the density-matrix in one common evolution-operator,

$$S_C(z, z') = \mathcal{T}_C \exp(-i\int_{z'}^{z} dz'' V(z'')), \tag{2.27}$$

where z and z' are unspecified points on the contour. Finally we can write the average of an observable as:

$$\langle O(s)\rangle = \frac{Z_0}{Z}\langle \mathcal{T}_C[S_C O(s)]\rangle_0 \text{ with } \langle ...\rangle_0 = \mathrm{Tr}(\rho_0 ...). \tag{2.28}$$

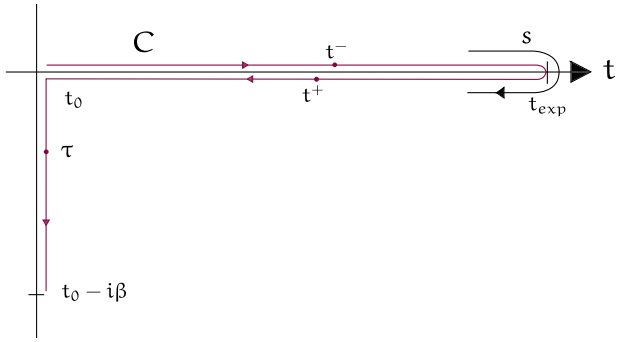

Figure 3: The full contour C that enables us to cover imaginary-time evolution and real-time-evolution on a common footing. t^- is a time on the forward branch, t^+ is a time on the backward branch and τ is a time on the imaginary branch. This contour is parametrized by the contour-time s, that runs from 0 to t_{exp} on the forward contour, from t_{exp} to $2t_{exp}$ on the backward contour and from $2t_{exp}$ to $2t_{exp} + \beta$ on the imaginary branch.

Again we have introduced a time-variable s living on the contour which is now from the interval $[0, 2t_{exp} + \beta]$. One can easily extend the theory above to correlation-functions with two times, such as the contour-ordered Green's function, which is defined on the contour as:

$$\begin{aligned} G_{a,b}(z,z') &= \langle T_C S_C c_a^\dagger(z) c_b(z') \rangle_0 \\ &= \langle S_C c_a^\dagger(z) c_b(z') \rangle_0 \Theta(z,z') - \langle S_C c_b(z') c_a^\dagger(z) \rangle_0 \Theta(z',z) \\ &= G^<(z,z')\Theta(z,z') - G^>(z,z')\Theta(z',z). \end{aligned} \tag{2.29}$$

We have defined the Θ-function on the contour as usual:

$$\begin{aligned} \Theta(z_1,z_2) &= 1 \text{ if } z_1 \text{ is later on C as } z_2 \\ &= 0 \text{ if } z_2 \text{ is later on C as } z_1. \end{aligned} \tag{2.30}$$

That means that if z is parametrized according to a linear $z(s)$ like it is given in (4.25) then $\Theta(z_1,z_2) = \Theta(z(s_1), z(s_2))$ reduces to $\Theta(s_1 - s_2)$.

Now we have a theory that seems to encompass everything we wished for:

- initial correlations can be treated,
- time-dependent problems can be treated,
- no reference to a state in the future is made.

But as there's no such thing as a free lunch, we pay for this with a complicated structure of the theory that for the moment is hidden in the time-ordered exponential.

Before we're going to derive equations that allow us to actually calculate something we cast the above theory into a functional framework.

2.4 A FUNCTIONAL APPROACH

We start with a partition function into which we introduced an artificial time-dependency [38, 39, 10]:

$$Z = \mathrm{Tr}(\rho U(0, t_{exp}) U(t_{exp}, 0)) \tag{2.31}$$

All evolution-operators can use the same Hamiltonian if one restricts the real-time evolution to the real axis via suitable Θ-functions.

where we use again a thermal density-matrix, $\rho = e^{-\beta H}$, and the time-evolution-operator is only on the real-axis for now. Similarly to eq. (2.24)) we can rewrite the thermal density-matrix:

$$Z = \mathrm{Tr}(\rho_0 U(-i\beta, 0) U(0, t_{exp}) U(t_{exp}, 0)). \tag{2.32}$$

With that and the picture of the full contour(Figure 3) in mind we can start to construct a functional expression. We subdivide the interval $[0, 2t_{exp} + \beta]$ in infinitesimal parts δ and insert a time-evolution-operator between every two time-slices. Note, as there's no evolution on the points of turn-around(t_{exp} and $2t_{exp}$ which corresponds to 0) we insert the unity instead. To work with a concrete example we split up each branch of the real-time axis in 3 parts and the imaginary part of the contour in two parts. Then we rewrite the partition function as

$$Z = \mathrm{Tr}[U^i U^i \mathbb{1} U^+ U^+ U^+ \mathbb{1} U^- U^- U^-] \tag{2.33}$$

where

- U^- is evolution about an infinitesimal on the forward branch.
- U^+ is evolution about an infinitesimal on the backward branch.
- U^i is evolution about an infinitesimal on the imaginary axis.

For the unfamiliar notation see Appendix A.

j corresponds to the index of the time-slice.

Next we insert a representation of the unity in the fermion coherent-state basis (A.1) between every time-evolution-operator and rewrite the trace as a functional integral (A.2), which leads us to:

$$\begin{aligned} Z = \int \prod_{j=0}^{9} d\bar{j} dj e^{-\bar{j}j} \langle -0|U^i|1\rangle\langle 1|U^i|2\rangle\langle 2|\mathbb{1}|3\rangle\langle 3|U^+|4\rangle\langle 4|U^+|5\rangle \cdot \\ \cdot \langle 5|U^+|6\rangle\langle 6|\mathbb{1}|7\rangle\langle 7|U^-|8\rangle\langle 8|U^-|9\rangle\langle 9|U^-|0\rangle. \end{aligned} \tag{2.34}$$

The expression on the left and right of the $\approx$ are related by the Trotter-decomposition.[38]

Next we must determine the action of the time-evolution-operator between two time-slices. For a normal-ordered Hamiltonian it is

$$\begin{aligned} \langle j|U^\delta|j+1\rangle &= \langle j|e^{-iH(c^\dagger, c)\delta}|j+1\rangle \approx e^{-iH(\bar{j}, j+1)\delta}\langle j|j+1\rangle \\ &= e^{-iH(\bar{j}, j+1)\delta} e^{\bar{j}(j+1)}. \end{aligned} \tag{2.35}$$

It's $+\delta$ on C^- because e^{-itH} is the forward *evolution*

We can handle the time-evolution on those different contour-parts in a unified manner, if we agree to lump this information together with the delta:

$$\delta = \begin{cases} +\delta & \delta \in C^- \\ -\delta & \delta \in C^+ \\ -i\delta & \delta \in C^i. \end{cases} \tag{2.36}$$

That way we get for the partition function of our example

$$\begin{aligned} Z = \int \prod_{j=0}^{9} d\bar{j} j e^{-\bar{j}j} e^{-\overline{(0)}(1) - i\delta H(-\bar{0}, 1)} e^{\overline{(1)}(2) - i\delta H(\bar{1}, 2)} e^{\overline{(3)}(4) - i\delta H(\bar{3}, 4)} \\ e^{\overline{(4)}(5) - i\delta H(\bar{4}, 5)} e^{\overline{(5)}(6) - i\delta H(\bar{5}, 6)} e^{\overline{(1)}(2) - i\delta H(\bar{1}, 2)} e^{\overline{(7)}(8) - i\delta H(\bar{7}, 8)} \\ e^{\overline{(8)}(9) - i\delta H(\bar{8}, 9)} e^{\overline{(9)}(0) - i\delta H(\bar{9}, 0)} e^{\overline{(2)}(3)} e^{\overline{(6)}(7)}. \end{aligned} \tag{2.37}$$

The powers of the exponentials get merged in the action S

$$Z = \int \prod_{j=0}^{9} d\bar{j} dj e^{S(\ldots,\bar{j},j,\ldots)}. \tag{2.38}$$

As the Hamiltonian is assumed to be separable in the non-interacting part H_0 and the interaction V, we can separate the action into the gaussian part

$$\begin{aligned} S_0 = &\sum_{j=0}^{9} (-\bar{j}j) - \overline{(0)}(1) - i\delta H_0(-\bar{0}, 1) + \overline{(1)}(2) - i\delta H_0(\bar{1}, 2) + \overline{(3)}(4) \\ &- i\delta H_0(\bar{3}, 4) + \overline{(4)}(5) - i\delta H_0(\bar{4}, 5) + \overline{(5)}(6) - i\delta H_0(\bar{5}, 6) + \overline{(1)}(2) \\ &- i\delta H_0(\bar{1}, 2) + \overline{(7)}(8) - i\delta H_0(\bar{7}, 8) + \overline{(8)}(9) - i\delta H_0(\bar{8}, 9) + \overline{(9)}(0) \\ &- i\delta H_0(\bar{9}, 0) + \overline{(2)}(3) + \overline{(6)}(7) \end{aligned} \tag{2.39}$$

and the interaction part

$$S_1 = \sum_{j=0}^{9} -i\delta_j V(\bar{j}, j+1). \tag{2.40}$$

Let's take a closer look at the gaussian part of the action S_0. Being quadratic we can represent it by a matrix:

$$\begin{pmatrix} \bar{0} \\ \bar{1} \\ \bar{2} \\ \bar{3} \\ \bar{4} \\ \bar{5} \\ \bar{6} \\ \bar{7} \\ \bar{8} \\ \bar{9} \end{pmatrix}^T \begin{pmatrix} -1 & \mu^i & & & & & & & & \\ & -1 & m^i & & & & & & & \\ & & -1 & 1 & & & & & & \\ & & & -1 & m^- & & & & & \\ & & & & -1 & m^- & & & & \\ & & & & & -1 & m^- & & & \\ & & & & & & -1 & 1 & & \\ & & & & & & & -1 & m^+ & \\ & & & & & & & & -1 & m^+ \\ m^+ & & & & & & & & & -1 \end{pmatrix} \begin{pmatrix} 0 \\ 1 \\ 2 \\ 3 \\ 4 \\ 5 \\ 6 \\ 7 \\ 8 \\ 9 \end{pmatrix} \tag{2.41}$$

with $m^l = -i\hat{e}\delta^l + 1$, $\mu^i = -i\hat{e}\delta^i - 1$ and $\hat{e}$ is a matrix that contains all eigenvalues of the free Hamiltonian on its diagonal. We identify the following structure in this expression:

Here we use the $\vec{\phi}_j$ notation to better see the structure in the time-index j.

$$\begin{aligned} \vec{\bar{\phi}}_j G_0^{-1} \vec{\phi}_{j+1} &= -\vec{\bar{\phi}}_j \phi_j + \vec{\bar{\phi}}_j (-i\delta\hat{e} + 1)\vec{\phi}_{j+1} \\ &= \delta(\vec{\bar{\phi}}_j \frac{\vec{\phi}_{j+1} - \vec{\phi}_j}{\delta} - i\vec{\bar{\phi}}_j \hat{e}\vec{\phi}_{j+1}). \end{aligned} \tag{2.42}$$

This means that a continuum-representation of the above matrix is

$$G_0^{-1} = \partial_z - iH_0 \tag{2.43}$$

where we've introduced the free propagator G_0^{-1}. With that we have all parts for taking the continuum's limit that allows us to write the partition function as a functional integral

$$Z = \int D[\vec{\bar{\phi}}(z), \vec{\phi}(z)] e^{S[\vec{\bar{\phi}}(z), \vec{\phi}(z)]} \tag{2.44}$$

where the action S is

$$\begin{aligned} S[\vec{\bar{\phi}}(z),\vec{\phi}(z)] &= \int_C dz\vec{\bar{\phi}}(z)G_0^{-1}\vec{\phi}(z) - i\int_C dz V[\vec{\bar{\phi}}(z),\vec{\phi}(z)] \\ &= S_0 + S_1 \end{aligned} \tag{2.45}$$

If you evaluate these integrals, you have to introduce a parametrization of the contour C, e.g. z(s)(most likely sth. piecewise linear) as in (4.25).

and the integrals run along our contour C. The information on which part of the contour we evaluate is now stored in the differential dz. If we introduce the averaging with the gaussian part

$$\langle\bullet\rangle_0 = \frac{1}{Z_0}\int D[\vec{\bar{\phi}}(z),\vec{\phi}(z)]e^{S_0[\vec{\bar{\phi}}(z),\vec{\phi}(z)]}\bullet \tag{2.46}$$

we can interpret the partition function as an averaging of the interaction with the free part:

$$\begin{aligned} Z &= \int D[\vec{\bar{\phi}}(z),\vec{\phi}(z)]e^{S_0[\vec{\bar{\phi}}(z),\vec{\phi}(z)]+S_1[\vec{\bar{\phi}}(z),\vec{\phi}(z)]} \\ &= Z_0\langle e^{S_1[\vec{\bar{\phi}}(z),\vec{\phi}(z)]}\rangle_0. \end{aligned} \tag{2.47}$$

For more details, take a look in [27].

We are also able to rewrite the partition function as a generating functional,

$$Z[\vec{J},\vec{\bar{J}}] = \int\int D[\vec{\bar{\phi}}(z),\vec{\phi}(z)]e^{S_0(\vec{\bar{\phi}}(z),\vec{\phi}(z))+S_1(\vec{\bar{\phi}}(z),\vec{\phi}(z))+i\vec{J}\vec{\phi}(z)-i\vec{\bar{\phi}}(z)\vec{\bar{J}}} \tag{2.48}$$

from which correlation-functions can be generated by functional derivation. From eq. (2.47) we can write down the expansion of the partition function

The parametrization z(s) takes care of the book-keeping of the phase-factors.

$$Z = Z_0\sum_{n=0}^{\infty}\frac{(-i)^n}{n!}\int_C dz_1 ... \int_C dz_n\langle V(z_1)V(z_2)....V(z_n)\rangle_0. \tag{2.49}$$

The one-particle Green's function can be generated via differentiating eq. (2.48) twice with respect to the source,

$$\begin{aligned} G_{a,b}(z,z') &= \frac{\delta^2 Z[\vec{J},\vec{\bar{J}}]}{\delta\bar{J}_a\delta J_b}\Big|_{J,\bar{J}=0} \\ &= \frac{1}{Z}\int D[\vec{\bar{\phi}}(z),\vec{\phi}(z)]e^{S(\vec{\bar{\phi}}(z),\vec{\phi}(z))}\overline{\phi}_a(z)\phi_b(z') \\ &= \langle\mathbb{T}_C c_a^\dagger(z)c_b(z')\rangle \end{aligned} \tag{2.50}$$

This is an aid for debugging. Note also, that observables are at least continuous at the turn-around points.

and in the last line we can make the connection to the canonical formulation of the previous chapter. Notice that the real-time branches are physically indistinguishable, thus for any operator holds $A(t^+) = A(t^-)$. Analogous to the partition function we expand the Green's function:

$$G_{a,b}(s,s') = \frac{Z_0}{Z}\sum_{n=0}^{\infty}\frac{(-i)^n}{n!}\int_C dz_1\dots dz_n\langle V(z_1)\dots V(z_n)\overline{\phi_a}(s)\phi_b(s')\rangle_0. \tag{2.51}$$

Wicks theorem can be easily derived in the functional approach, being a property of gaussian integrals[27]. A derivation in the canonical formulation is also possible [8, 9]. Having now stated the theory in a canonical formulation and in the functional framework we need to derive equations of motions for eventually performing calculations.

3 EQUATIONS OF MOTION

$$\vec{F} = \frac{d\vec{p}}{dt}$$

— *Isaac Newton*

Back in eq. (2.27) we arrived at an equation for the time-evolution that's not totally unlike the expression known from Feynman-, or Matsubara-theory. Similarly it satisfies equations of motions

H_z *means that the Hamiltonian* H *has a time-dependency in the Schrödinger-picture.*

$$i\frac{\partial}{\partial z}U(z,z') = H_z U(z,z') \tag{3.1}$$

$$-i\frac{\partial}{\partial z'}U(z,z') = U(z,z')H_z \tag{3.2}$$

$$\tag{3.3}$$

with the initial condition $U(z,z) = \mathbb{1}$. Starting from the connection between Schrödinger- and Heisenberg-operators

$$A_H(z) = U(0,z)A_S(z)U(z,0) \tag{3.4}$$

we can derive the equation of motion for Heisenberg-operators

$$\frac{d}{dz}A_H(z) = i[H_z, A_S(z)]_H(z) + (\frac{dA_S(z)}{dz})_H \tag{3.5}$$

with the initial condition $A_H(0) = A_S(0)$. Equipped with these relations we want to derive equations of motion for the Green's function [13]. From eq. (3.5) we infer that for the annihilator the equation

$$i\frac{d}{dz}c_a(z) = [H_z, c_a]_H(z) \tag{3.6}$$

and similarly for the adjungated operator holds. For the time-ordered Green's function(2.29) we end up with

The relation $\frac{d}{dz}\Theta(z,z') = \delta(z,z')$ *is assumed with* δ *being the Dirac-*δ *function.*

$$\frac{d}{dz}G_{a,b}(z,z') = \delta(z,z')\delta_{a,b} + i\langle \mathbb{T}_C[H_z, c_a^\dagger]_H(z)c_b(z')\rangle \tag{3.7}$$

and similarly

$$\frac{d}{dz'}G_{a,b}(z,z') = -\delta(z,z')\delta_{a,b} + i\langle \mathbb{T}_C c_a^\dagger(z)[H_z, c_b]_H(z')\rangle. \tag{3.8}$$

If we restrict $z(s)$ to certain parts of the contour we can derive differential equations on linear parts of the contour [13]. For the real-time lesser and greater Green's functions we get

From now on, all operators are in the Heisenberg-picture.

The δ*s vanish because* $G^{</>/\lceil/\rceil}$ *are defined having their times on completely different branches of the contour.*

$$\frac{d}{dt}G^<_{a,b}(t,t') = -i\langle c_b(t')[H_t, c_a^\dagger](t)\rangle \tag{3.9}$$

$$\frac{d}{dt'}G^<_{a,b}(t,t') = -i\langle [H_t, c_b](t')c_a^\dagger(t)\rangle \tag{3.10}$$

$$\frac{d}{dt}G^>_{a,b}(t,t') = i\langle [H_t, c_a^\dagger](t), c_b(t')\rangle \tag{3.11}$$

$$\frac{d}{dt'}G^>_{a,b}(t,t') = i\langle c_a^\dagger[H_t, c_b](t')\rangle \tag{3.12}$$

with the initial condition $G^{>}(0,0) = \lim_{\eta\to 0} G^{M}(-i\eta, 0)$ and $G^{<}(0,0) = \lim_{\eta\to 0} G^{M}(0,-i\eta)$. For these two Green's functions the relation

$$\left[G^{\lessgtr}(t,t')\right]^{\dagger} = -G^{\lessgtr}(t',t) \tag{3.13}$$

holds.

Next there are the Green's functions that have exactly one time-variable on the imaginary-axis

$$\frac{d}{dt}G^{\rceil}_{a,b}(t,\tau) = \quad -i\langle c_b(\tau)[H_t, c_a^{\dagger}](t)\rangle \tag{3.14}$$

$$\frac{d}{dt}G^{\lceil}_{a,b}(\tau,t) = \quad i\langle c_a^{\dagger}(\tau)[H_t, c_b](t)\rangle \tag{3.15}$$

Note that τ is an imaginary number.

where the initial-conditions are given by the Matsubara Green's function: $G^{\rceil}(0,\tau) = G^{M}(0,\tau)$ and $G^{\lceil}(\tau,0) = G^{M}(\tau,0)$. $G^{\lceil}$ and $G^{\rceil}$ are related by [14]:

$$G^{\rceil}(\tau,t) = (G^{\lceil})^{\dagger}(t,\beta-\tau). \tag{3.16}$$

And finally there's the Matsubara Green's function with both of its time-arguments on the imaginary axis.

$$\frac{d}{d\tau}G^{M}_{a,b}(\tau,\tau') = \quad \delta(\tau-\tau')\delta_{ab} + \langle \mathbb{T}_{\tau}[H_{\tau}, c_a^{\dagger}](\tau)c_b(\tau')\rangle \tag{3.17}$$

$$\frac{d}{d\tau'}G^{M}_{a,b}(\tau,\tau') = \quad -\delta(\tau-\tau')\delta_{ab} + \langle \mathbb{T}_{\tau}c_a^{\dagger}(\tau)[H_{\tau}, c_b](\tau')\rangle. \tag{3.18}$$

These equations have to be solved with respect to the Kubo-Martin-Schwinger-Boundary-conditions $G^{M}(\tau+i\beta,\tau') = -e^{\beta\mu N}G^{M}(\tau,\tau')$. In the literature there's a bunch of more powerful methods to solve for the Matsubara Green's function than solving the differential equation (3.18) directly [2, 40, 41].

Part II

THE ALGORITHM

4 QUANTUM MONTE-CARLO

We have seen that computer programming is an art,
because it applies accumulated knowledge to the world,
because it requires skill and ingenuity, and especially
because it produces objects of beauty.

— Donald E. Knuth [42]

4.1 MONTE-CARLO METHODS

Basic probability theory states that the expectation value of an observable, denoted by $\langle O \rangle$, is given by

$$\langle O \rangle = \sum_i F(x_i) O(x_i) \tag{4.1}$$

where the sum runs over all discrete states x_i of the system. The value of the observable for a given state is determined, hence $O(x_i)$ is calculated, and multiplied by the weight $F(x_i)$ of the state. The idea is then, to generate a series of microscopic states x_i according to the distribution-function $F(x_i)$. That way, states with a large weight in the distribution function are generated with a larger probability than those with a small weight. One method is to use a suitable Markov-chain for that task. The new configurations don't get drawn at random but according to the distribution-function F. A Markov-process that generates a chain of states $\{x_n\}$ defines the rules of the transition from a given initial state x_i to the next state x_{i+1}. That is the transition from x_i to x_{i+1} happens with a certain probability $P_{x_i \to x_{i+1}}$. The following state is then determined according to the same rules. We can already deduce some properties of these probabilities.

As the Markov-process generates the new state only from the preceding state, it has no memory of how it got there.

- $P_{x_i \to x_{i+1}}$ must have an interpretation as probability, hence

$$P_{x_i \to x_{i+1}} \geqslant 0 \ \forall x_i, x_{i+1}. \tag{4.2}$$

This first property leads in QMC simulations to the problem known as the fermionic sign problem.

- The probability of getting in *any* subsequent state must be normalized

$$\sum_{x_{i+1}} P_{x_i \to x_{i+1}} = 1. \tag{4.3}$$

Further we expect the Markov-process to have a stationary distribution that coincides with the desired distribution F. Having reached that distribution, we want to stay there, that is

$$\sum_{x_i} F(x_i) P_{x_i \to x_{i+1}} = F(x_{i+1}) \ \forall x_{i+1}. \tag{4.4}$$

For the actual construction of the Markov-chain it is easier to demand that the so called *detailed balance* condition holds:

$$F(x_i) P_{x_i \to x_{i+1}} = F(x_{i+1}) P_{x_{i+1} \to x_i}. \tag{4.5}$$

Summing (4.5) over x_i, it can be proven that this condition satisfies stationarity. To progress further we split the transition probability P into two parts.

- The new state x_{i+1} is proposed with proposal probability $T_{x_i \to x_{i+1}}$.
- Then it is accepted with the probability of acceptance $A_{x_i \to x_{i+1}}$.

That way we have

$$P_{x_i \to x_{i+1}} = T_{x_i \to x_{i+1}} A_{x_i \to x_{i+1}}. \tag{4.6}$$

Inserting this into (4.5) we have

$$F(x_i) T_{x_i \to x_{i+1}} A_{x_i \to x_{i+1}} = F(x_{i+1}) T_{x_{i+1} \to x_i} A_{x_{i+1} \to x_i}. \tag{4.7}$$

With the definition of the ratio

$$Z_{x_i, x_{i+1}} = \frac{T_{x_{i+1} \to x_i} F(x_{i+1})}{T_{x_i \to x_{i+1}} F(x_i)} \tag{4.8}$$

and the assumption that the acceptance probabilities have a functional form that depends only on $Z_{x_i, x_{i+1}}$, that is

$$A_{x_i \to x_{i+1}} = \Phi(Z_{x_i, x_{i+1}}),$$

we can rewrite eq. (4.5) as

$$\frac{\Phi(Z)}{\Phi(\frac{1}{Z})} = Z \tag{4.9}$$

with Z an abbreviation for $Z_{x_i, x_{i+1}}$. Φ should map any positive value to a probability, hence

$$\Phi : (0, \infty) \to [0, 1]. \tag{4.10}$$

Now the only thing left to us, is specifying the function Φ. The most popular choice is the one of Metropolis,

$$\Phi(Z) = \min(1, Z). \tag{4.11}$$

Another possible choice is the so-called Heat-Bath-algorithm with

$$\Phi(Z) = \frac{Z}{1 + Z}. \tag{4.12}$$

In an implementation we would first draw a random number r from the interval $[0, 1]$. Then if $r < \Phi(Z)$ one accepts the proposed move x_{i+1}, else the move is rejected. That way we generate a Markov-Chain of states $x_i, i \in \{1, ..., N\}$ of length N where each state x_i is distributed according to the distribution function $F(x_i)$. One has to take care that initially the Markov-process has not yet relaxed to its stationary distribution F, thus one has to include a certain warm-up time. Having these states x_i we can start the measurement of observables. The resulting Monte-Carlo estimate of the observable is the average over all generated states:

$$\langle O \rangle_{MC} = \frac{1}{N} \sum_i O(x_i). \tag{4.13}$$

In case the central limit theorem holds the standard-deviation gives the error according to $\Delta O = \sigma_O / \sqrt{N}$. But there's the catch, for the central limit theorem to be applicable we need a large number of *uncorrelated* measurements. But having generated the states x_i via a small local change to the preceding states, the different measurements of the observables are of course correlated. Lacking the central limit theorem, other types of estimators for observables have to be used, e.g. the Jackknife-method or the Bootstrap method [43].

4.2 DDQMC ON THE CONTOUR

For deriving a Markov-chain Quantum-Monte-Carlo as outlined in the previous section we need the transition-probabilities between different configurations. Starting from the partition function we derive a DDQMC method on the full contour(remember Figure 3) similar as done in [44, 40, 33] on the imaginary contour. For that we recall the expression of the partition function on the contour, eq. (2.49)

$$Z = Z_0 \sum_{n=0}^{\infty} \frac{(-i)^n}{n!} \int_C dz_1 ... \int_C dz_n \langle \mathbb{T}_C V(z_1)V(z_2)....V(z_n)\rangle_0. \quad (4.14)$$

In the following we assume that we are looking at Hubbard-like models, hence the interaction-part is

$$H_U = U \sum_i (n_{i,\uparrow} - \frac{1}{2})(n_{i,\downarrow} - \frac{1}{2}) \quad (4.15)$$

with $n_{i,\sigma}$ being the particle density of species σ on site i.

Similar as in [44] we introduce an additional Ising spin s^i in the interaction

$$H_U = \frac{U}{2} \sum_i \sum_{s^i=\pm 1} (n_{i,\uparrow} - \frac{1}{2} - s^i\delta)(n_{i,\downarrow} - \frac{1}{2} + s^i\delta) \quad (4.16)$$

where we have introduced the new parameter δ. δ is an additional factor to the partition function but it doesn't influence the measurement of physical observables, where it is equally occurring in the denominator and the nominator. From thermodynamic QMC it is known that δ can be used to reduce the sign-problem of the simulation. The usual choice for 1D Hubbard-models to eliminate the sign-problem is $\delta = \frac{1}{2} + 0^+$. Introducing that into the general expansion for the partition function (4.14) gives

We will show in the application-part, that at least for particle-hole symmetric chains $\delta \to 0$ reduces the dynamic sign problem of the real-time evolution.

$$\frac{Z}{Z_0} = \sum_{n=0}^{\infty} \frac{\left(\frac{-iU}{2}\right)^n}{n!} \int_C dz_1 \sum_{i_1,s^1} \dots \int_C dz_n \sum_{i_n,s^n} \prod_\sigma \langle \mathbb{T}_C (n_{i_1,\sigma}(z_1) - \alpha_{\sigma,s^1}) \dots (n_{i_n,\sigma}(z_n) - \alpha_{\sigma,s^n})\rangle_0 \quad (4.17)$$

where we have introduced

$$\alpha_{\sigma,s^i} = \frac{1}{2} + \sigma s^i \delta \quad (4.18)$$

and made use of the fact that for SU(2) - symmetric problems the weight splits up in an $\uparrow$-part and a $\downarrow$ - part. We can compactify (4.17) by introducing *configurations*. A configuration consists of Hubbard-vertices with their Ising-spin $V_j = [i_j, z_j, s^j]$, that is

$$C_n = \{[i_1, z_1, s^1], \dots, [i_n, z_n, s^n]\}. \quad (4.19)$$

With that concept we can introduce the sum over the configuration-space

$$\sum_{C_n} = \sum_{n=0}^{\infty} \frac{1}{n!} \int_C dz_1 \sum_{i_1,s^1} \dots \int_C dz_n \sum_{i_n,s^n}. \quad (4.20)$$

With that (4.17) can be rewritten as

$$\frac{Z}{Z_0} = \sum_{C_n} \left(-i\frac{U}{2}\right)^n \prod_\sigma \langle \mathbb{T}_C (n_{i_1,\sigma}(z_1) - \alpha_{\sigma,s^1}) \dots (n_{i_n,\sigma}(z_n) - \alpha_{\sigma,s^n})\rangle_0. \tag{4.21}$$

Using Wick's theorem, the time-ordered average in the above equation can be rewritten as a determinant,

$$\begin{aligned}
&\langle \mathbb{T}_C (n_{i_1,\sigma}(z_1) - \alpha_{\sigma,s^1}) \dots (n_{i_n,\sigma}(z_n) - \alpha_{\sigma,s^n})\rangle_0 = \\
&\begin{vmatrix}
G^0_{i_1,i_1}(z_1,z_1) - \alpha_{\sigma,s^1} & G^0_{i_1,i_2}(z_1,z_2) & \cdots & G^0_{i_1,i_n}(z_1,z_n) \\
G^0_{i_2,i_1}(z_2,z_1) & G^0_{i_2,i_2}(z_2,z_2) - \alpha_{\sigma,s^2} & \cdots & G^0_{i_2,i_n}(z_n,z_n) \\
\vdots & \vdots & & \vdots \\
G^0_{i_n,i_1}(z_n,z_1) & G^0_{i_n,i_2}(z_n,z_2) & \cdots & G^0_{i_n,i_n}(z_n,z_n) - \alpha_{\sigma,s^n}
\end{vmatrix} \\
&= \det(M_\sigma(C_n)).
\end{aligned} \tag{4.22}$$

The entries of $M_\sigma(C_n)$ are given by the free Green's function

$$M(C_n)_{i,k} = G^{(0)}_{i,k}(z_i, z_k) = \langle \mathbb{T}_C c^\dagger_i(z_i) c_k(z_k)\rangle_0. \tag{4.23}$$

With all this, the partition function (4.21) can be cast in a rather convenient form

$$\frac{Z}{Z_0} = \sum_{C_n} \left(-\frac{iU}{2}\right)^n \prod_\sigma \det(M_\sigma(C_n)). \tag{4.24}$$

For the Monte-Carlo evaluation of the contour-integrals in (4.20) we have to transform them to linear integrals. To achieve that we need to specify the parametrization of the contour, and we choose the most obvious linear one:

$$z(s) = \begin{cases} s & s \in [0, t_{exp}] \\ 2t_{exp} - s & s \in (t_{exp}, 2t_{exp}] \\ -i(s - 2t_{exp}) & s \in (2t_{exp}, 2t_{exp} + \beta]. \end{cases} \tag{4.25}$$

Now you have to replace every contour-integral by

$$\int_C dz \cdots = \int_0^L ds \cdot \frac{dz(s)}{ds} \dots \tag{4.26}$$

with the contour-length $L = 2t_{exp} + \beta$. This phase-factor $\frac{dz(s)}{ds}$ can, because of relation (4.25), take the values $1, -1, -i$. With these notations we can deduce the weight of a configuration from the partition function (4.24)

Note, that in real-time evolution the weight is usually a complex value.

$$W(C_n) = \left(\frac{-iU}{2}\right)^n \prod_\sigma \det(M_\sigma(C_n)) F(C_n) \tag{4.27}$$

where $F(C_n)$ collects the contribution from all phases in the configuration:

$$F(C_n) = \prod_{k=0}^n \frac{dz(s)}{ds}\bigg|_{s=s_k}. \tag{4.28}$$

For the Markov-process as outlined above we need, additionally to the weights, the proposal probabilities for the moves. The addition of a vertex is proposed with $T_{C_n \to C_{n+1}} = \frac{1}{2NL}$, which corresponds to the selection of a spin(there are two of them), the choice of a site(from N sites) and of a contour-time in the range from $[0, 2t_{exp} + \beta]$. The proposal probability to remove a vertex is $T_{C_{n+1} \to C_n} = \frac{1}{n+1}$ which corresponds to the selection of a vertex from C_{n+1} which has $n+1$ vertices. Now we would like to write down the moves for the Metropolis-algorithm but we encounter the problem that G^0 is an arbitrarily complex value and, additionally, the expressions for the weights have imaginary units all over them. So we can't interpret these weights as probabilities (see (4.2)). The solution is that instead of working with the weights $W(C_n)$ we use their absolute values $|W(C_n)|$, but we have to fix this up later when measuring observables by keeping track of the phase of a configuration. We write down the moves with the imaginary units still intact, keeping in mind that while implementing them we have to use the absolute values:

Note that playing with the weights means an alteration of the stationary distribution of the Markov-process!

$$P_{C_n \to C_{n+1}} = \min\left(\frac{-iUNLF(C_{n+1}) \prod_\sigma \det(M_\sigma(C_{n+1}))}{(n+1)F(C_n) \prod_\sigma \det(M_\sigma(C_n))}, 1\right) \quad (4.29)$$

and

$$P_{C_{n+1} \to C_n} = \min\left(\frac{(n+1)F(C_n) \prod_\sigma \det(M_\sigma(C_n))}{-iUNLF(C_{n+1}) \prod_\sigma \det(M_\sigma(C_{n+1}))}, 1\right). \quad (4.30)$$

Theses two moves are usually sufficient for the ergodicity of the algorithm. See [44] for a discussion of the cases where this doesn't apply.

4.3 MEASURING OBSERVABLES

Having generated the Markov - chain of configurations we can start to measure observables, e.g. Green's functions. Having already an expansion for the Green's function (2.51) we can start rewriting it as a sum over all configurations:

$$\begin{aligned} G_{ij}(s,s') &= \frac{Z_0}{Z} \sum_{n=0}^{\infty} \frac{(-i)^n}{n!} \int_C dz_1 \dots dz_n \langle \mathbb{T}_C H_U(z_1) \dots H_U(z_n) c_i^\dagger(z(s)) c_j(z(s')) \rangle_0 \\ &= \frac{\sum_{C_n} \left(-\frac{iU}{2}\right)^n F(C_n) \prod_\sigma \det(M_\sigma(C_n)) \langle\langle G_{ij}(s,s') \rangle\rangle_{C_n}}{\sum_{C_n} \left(-\frac{iU}{2}\right)^n F(C_n) \prod_\sigma \det(M_\sigma(C_n))} \\ &= \frac{\sum_{C_n} W(C_n) \langle\langle G_{ij}(s,s') \rangle\rangle_{C_n}}{\sum_{C_n} W(C_n)} \end{aligned} \quad (4.31)$$

where we have similarly to [44] introduced the contribution of one configuration to the observable

$$\langle\langle G_{ij}(s,s') \rangle\rangle_{C_n} = \frac{\langle \mathbb{T}_C H_U(z_1) \dots H_u(z_n) c_i^\dagger(z(s)) c_j(z(s')) \rangle_0}{\langle \mathbb{T}_C H_U(z_1) \dots H_u(z_n) \rangle_0}. \quad (4.32)$$

Now we can see the connection to the Markov-process in Section 4.1. The weight of a configuration $W(C_n)$ takes the role of the probability density F in (4.1).

Now we are at the right spot to elaborate a bit on the sign problem. As stated before we have to replace the true weight $W(C_n)$ by its absolute value $|W(C_n)|$. We can repair this by rewriting the last equation of (4.31) with $W(C_n) = |W(C_n)|\pi(C_n)$. We have introduced the phase-factor $\pi(C_n) = e^{i\arg(W(C_n))} = \frac{W(C_n)}{|W(C_n)|}$. Then

$$\begin{aligned} G_{ij}(s,s') &= \frac{\sum_{C_n} W(C_n)\langle\langle G_{ij}(s,s')\rangle\rangle_{C_n}}{\sum_{C_n} W(C_n)} \\ &= \frac{\sum_{C_n} |W(C_n)|\pi(C_n)\langle\langle G_{ij}(s,s')\rangle\rangle_{C_n}}{\sum_{C_n} |W(C_n)|\pi(C_n)}. \end{aligned}$$

expanding this fraction by $\frac{1}{\sum_{C_n}|W(C_n)|}$ gives:

$$\begin{aligned} &= \frac{\frac{\sum_{C_n} |W(C_n)|\pi(C_n)\langle\langle G_{ij}(s,s')\rangle\rangle_{C_n}}{\sum_{C_n}|W(C_n)|}}{\frac{\sum_{C_n} |W(C_n)|\pi(C_n)}{\sum_{C_n}|W(C_n)|}} \\ &= \frac{\langle \pi G_{ij}(s,s')\rangle}{\langle\pi\rangle}. \end{aligned} \tag{4.33}$$

That way we see that measuring physical observables requires keeping track of the phase-afflicted observable and of the phase itself. The average value of the true physical observable is then determined as their ratio.

For the reduction of higher Green's functions to single particle Green's functions see [40].

4.4 TESTS

Similarly to [44] we derive an equation for the average expansion order $\langle n\rangle$, as it is a quite useful milestone when writing and debugging the code. For a general interaction V the average expansion parameter $\langle n\rangle$ is given by

$$\begin{aligned} \langle n\rangle &= \frac{Z_0}{Z}\langle e^{S_1} n\rangle_0 \\ &= \frac{Z_0}{Z}\sum_n \frac{(-i)^n n}{n!}\int_C dz_1 ... \int_C dz_n \langle \mathbb{T}_C V(z_1)...V(z_n)\rangle_0 \\ &= \frac{-iZ_0}{Z}\sum_n \frac{(-i)^{n-1}}{(n-1)!}\int_C dz_1 ... \int_C dz_{n-1}\int_C dz_n \langle \mathbb{T}_C V(z_1)...V(z_{n-1})V(z_n)\rangle_0 \\ &= \frac{-iZ_0}{Z}\sum_k \frac{(-i)^k}{k!}\int_C dz_1 ... \int_C dz_k \int_C dz \langle \mathbb{T}_C V(z_1)...V(z_k)V(z)\rangle_0 \\ &= -i\int_C dz\langle V(z)\rangle. \end{aligned} \tag{4.34}$$

To further simplify, we assume that the interaction V is the same on the forward and backward branch $V(t^+) = V(t^-)$. Then we can simplify

$$\begin{aligned}\int_C dz\langle V(z)\rangle &= \int_0^{t_{exp}} dt^- V(t^-) + \int_{t_{exp}}^0 dt^+ V(t^+) - i\int_0^\beta d\tau V(\tau) \\ &= -i\int_0^\beta d\tau V(\tau)\end{aligned} \tag{4.35}$$

As the contributions of the real-time branches cancel, only the contribution of the imaginary time remains. That way we see, that the average expansion order is completely determined by the imaginary-time evolution of the system.

Part III

SELECTED APPLICATIONS

5 TESTS WITH TOY-MODELS

Debugging is twice as hard as writing
the code in the first place.
Therefore, if you write the code as cleverly as possible,
you are, by definition, not smart enough to debug it.

— Brian W. Kernighan

Having developed the theory and the algorithm in the previous parts, we apply this to 1D Hubbard-like models. The second quantized Hamiltonian of the fermionic Hubbard-Model is

$c, c^\dagger$ *of course fulfill fermionic commutation rules.*

$$H = -\sum_{ij\sigma} t_{ij} c^\dagger_{i\sigma} c_{j\sigma} + U \sum_i (n_{i\uparrow} - \frac{1}{2})(n_{i\downarrow} - \frac{1}{2}) \tag{5.1}$$

where $c_{i\sigma}$ annihilates an electron on site i with spin σ and $c^\dagger_{i\sigma}$ creates an electron on site i with σ being the z-component of the spin. U is a local Coulomb-interaction and we already assumed that the hopping-matrix t_{ij} is spin-independent. It is the simplest known model that allows to study the interplay of kinetic-energy, lattice-structure, Coulomb-interaction, Pauli's exclusion principle and doping(set via the chemical potential). A derivation from the general Hamiltonian of solid-state physics first neglects all dynamics of the lattice. Then it is assumed that at the relevant energy-scale around the Fermi-energy there is only one relevant energy-band, that is, the overlap between states of different bands is negligible. The Coulomb-interaction between electrons is reduced to its on-site matrix-element U, because the overlap of different atomic wave-functions with each other is assumed to be small [2]. Albeit simple in appearance and formulated already in 1963 [45] the general solution of the Hubbard-model is still not known. The Hubbard-model is the most prominent toy of many-particle physicists as being remarkable simple in appearance, it contains a good bunch of interesting physics. It is used to discuss

A solution in 1D can be derived via the Bethe-ansatz. See e.g. [30].

On increasing U, the electron-electron correlations increase and for some finite value the transition to an insulator occurs, because single-particle excitations get suppressed. The correlations force a transition from a correlated metal to a paramagnetic insulator [46].

- electronic properties of solids with narrow bands,
- transitions from metals to insulators, the Mott-transition,
- general properties of statistical mechanics,
- high-temperature super-conductivity in cuprate compounds.

The basic Hubbard model as sketched above is usually used as a many-particle physicists playground. To describe real-life materials the Hubbard model gets extended by additional terms or band-indices. Then there are a couple of examples of uses of the Hubbard-model in the literature [46]. It can be used to describe 1D polymer chains if extended with at least one additional nearest-neighbour interaction([47]) and some term that introduces a coupling to the nuclei. A comparison of organic salts with a description in terms of a Hubbard-model is done in [48]. The Hubbard-model was also used extensively to explain

magnetism in transition metals. Transition metals have quite narrow d-bands and the hopping and Coulomb matrix elements decay fast with distance. Thus the restriction to an on-site repulsion on its own would be well justified. But we can't restrict the model to a single band only as other bands are near in energy. This leads to the multi-band Hubbard-model with band-dependent interactions. [49] shows the necessity to work with a multiband Hubbard-model to explain the magnetic properties of these substances. An application of the multi-band Hubbard-model even found application at the description of the behaviour of doped fullerenes[50]. These different bands arise due to the number of doped atoms in the C_{60}-host. They show numerically that their model displays a Mott-transition using a Monte-Carlo technique. Theorists routinely claim that the Hubbard-model describes High Temperature Super Conductivity (HTSC) phenomena in cuprate compounds. The theoretical description starts often with the three-band Hubbard-model in two dimensions where the electron states are located on the Cu and O sites and an additional non-diagonal interaction is introduced between Cu and O; as outlined in [51]. Due to the large observed values of the electron-electron interaction in those materials they are believed to be highly correlated materials. It is established that magnetic excitations play a key role in the formation of Cooper pairs[52] in the cuprates. Recently it was observed that pair excitations already form before the onset of superconductivity [53]. Voroshilov [54] claims that this preforming of pairs can be derived in the framework of the 2D single band Hubbard-model. It is hoped that experiments with ultracold atoms can provide an insight on the properties of large Hubbard-like systems as they provide a clean environment for doing experiments ([55] explores this idea). The most recent numerically exact overview of the thermodynamic properties of the 2D Hubbard-model is given in [56]. Being an important physical model, the Hubbard model often finds use as a benchmark for new numerical methods [44].

In the following we restrict the discussion to nearest-neighbour hopping, that is $t_{ij} = t(\delta_{i+1,j} + \delta_{i-1,j})$ in one dimension. Also note that all time-scales have to be interpreted in units of the hopping-parameter t.

5.1 THE FREE GREEN'S FUNCTION OF THE 1D HUBBARD-MODEL

Being a perturbative method, the main ingredient of the DDQMC-algorithm is the free Green's function G^0; thus we need to calculate G^0 of the Hubbard-model on the contour. Via a Fourier-transform in the space-indices the free part H_0 can be transformed to the diagonal representation

$$H_0 = \sum_{k\sigma} \epsilon(k) c^\dagger_{k\sigma} c_{k\sigma} \tag{5.2}$$

with the spin-independent dispersion-relation $\epsilon(k) = -2t\cos(k)$, where we assumed the lattice-constant a to be 1 and have used periodic boundary conditions. We solve the Heisenberg-equation (3.5) for $c_q^\dagger$

$$\begin{aligned}\frac{d}{dz}c_q^\dagger(z) &= i[H_0, c_q^\dagger](z)\\ &= i[\sum_k \epsilon(k)c_k^\dagger c_k, c_q^\dagger](z)\\ &= i\sum_k \epsilon(k)[c_k^\dagger c_k, c_q^\dagger](z)\\ &= i\sum_k \epsilon(k)\delta_{qk}c_k^\dagger(z) = i\epsilon(q)c_q^\dagger(z)\end{aligned} \tag{5.3}$$

This ODE has the solution

$$c_q^\dagger(z(s)) = e^{i\epsilon(q)z(s)}c_q^\dagger \tag{5.4}$$

Note that the derivatives in these ODEs are not on a linear domain but on the contour C!

Analogously the result for the annihilator is

$$c_q(z(s)) = e^{-i\epsilon(q)z(s)}c_q \tag{5.5}$$

Now we can write down the free Green's function $G^{0,<}$ and $G^{0,>}$:

$$\begin{aligned}G^{0,<}_{k,k'}(s,s') &= \langle c_k^\dagger(s)c_{k'}(s')\rangle_0\\ &= e^{i(\epsilon(k)z(s)-\epsilon(k')z(s'))}\langle c_k^\dagger c_{k'}\rangle_0\end{aligned} \tag{5.6}$$

$$\begin{aligned}G^{0,>}_{k,k'}(s,s') &= \langle c_{k'}(s')c_k^\dagger(s)\rangle_0\\ &= e^{i(\epsilon(k)z(s)-\epsilon(k')z(s'))}\langle c_{k'}c_k^\dagger\rangle_0\end{aligned} \tag{5.7}$$

We're still missing one piece, that is $\langle c_k^\dagger c_{k'}\rangle$. But the solution is known [2] to be

$$\begin{aligned}\langle c_k^\dagger c_{k'}\rangle &= \delta_{k,k'}n_k\\ &= \delta_{k,k'}f(\epsilon(k)),\end{aligned} \tag{5.8}$$

with the Fermi-function

$$f(x) = \frac{1}{1+e^{\beta x}}. \tag{5.9}$$

Therefore we arrive at

$$G^{0,<}_{k,0}(s,s') = e^{i\epsilon(k)(z(s)-z(s'))}f(\epsilon(k)) \tag{5.10}$$

$$G^{0,>}_{k,0}(s,s') = e^{i\epsilon(k)(z(s)-z(s'))}(1-f(\epsilon(k))) \tag{5.11}$$

The contour-ordered Green's function, that is the major building-block for the expansion, is in the end:

$$G^0_k(s,s') = \Theta(s-s')G^{0,<}_k(s,s') - \Theta(s'-s)G^{0,>}_k(s,s') \tag{5.12}$$

Note that this Green's function has times in the contour-time s, thus you need to transform them via $z(s)$ to their physical times.

5.2 THE FREE TIME-DEPENDENT HUBBARD-MODEL

As a first step we chose not to include any explicit time-dependence, but look at the evolution of a system in thermal equilibrium. Setting $t_{exp} = 0$ we could check that our code was able to reproduce the thermodynamic properties of the Hubbard-chain, which was, surprisingly, the case. After this little milestone we increased the expansion time and we already know what should happen to the observables: Absolutely nothing, the system is in thermal equilibrium. All observables should have their thermodynamic values independent of the chosen expansion time t_{exp} (see Figure 10 for proof). Although we know that the observables don't change, there are still a couple of observables of interest, namely those specific to the Monte-Carlo process. These are the average sign $\langle s \rangle$ and the average length $\overline{n}$ of the generated configurations C_n, denoted by $\overline{n}(C_n)$. $\overline{n}$ may not be confused with the average expansion order from eq. (4.35)! $\langle n \rangle$ is the thermal average of a physical observable and thus is constant for all times, while $\overline{n}$ is determined by the peculiarities of the Monte-Carlo process and seems to grow proportional to t_{exp}. Because the single-site model shows some deviations in its distribution(Figure 6) we take a close look at that first and compare it to larger chains later. In Figure 4 we see the average configuration length of the single-site Hubbard-model. At $t_{exp} = 0$ we start out with the thermal value of the Configuration length of ≈ 0.16, and for times up to 5.3 the configuration length seems to increase linearly with t_{exp}. After that occur large jumps to 3 and 12 which are connected to sharp drops in the average sign(see figure 5). This is due to deviations from the gaussian shape of the distribution of $\bar{n}$(see Figure 6). The sign starts out at 1 and, in the special case of the 1-site

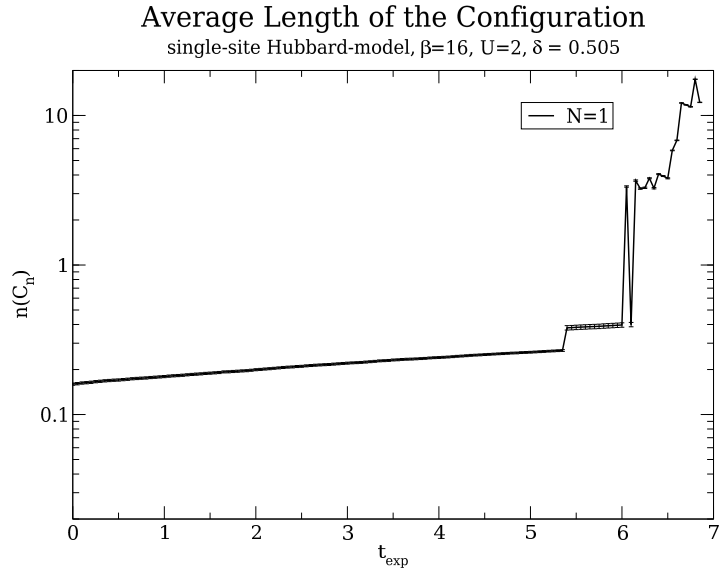

Figure 4: This is the average configuration length of the single site Hubbard-model. The Configuration length is plotted logarithmically against t_{exp}. Although having error-bars the figure should only be trusted up to ≈ 5.5, as beyond that, the simulation has problems of satisfying ergodicity.

model, decays rather slowly. At $t_{exp} \approx 6$ the sign drops and it drops even more around 6.4. The oscillating behaviour at these points is an artifact of the Monte-Carlo sampling of the distribution that now seems to have two peaks. Figure 6 shows that the distributions are centered at 0 and for larger times upto 5 the distribution only broadens a little bit. At around $t_{exp} = 5.5$ there are configurations with a significantly larger $\overline{n}$ (up to $\overline{n} = 30$ which is of course a long way off of the thermally expected 0.16) and at around $t_{exp} \approx 6$ the deviation from the initial distribution is clearly visible. It is not yet clear whether this is a genuine feature of the combined real-time and imaginary-time expansion that we use or some artifact of an imperfect Monte-Carlo sampling. Initially the distributions are centered at 0 and for larger times up

Very likely the simulation has also not yet thermalized, as it has a very hard time reaching that second emerging peak of the histogram.

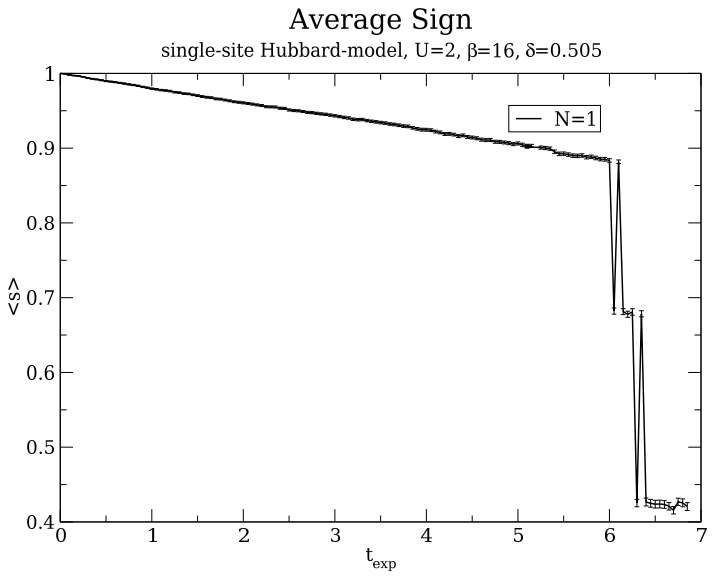

Figure 5: Average sign of the single-site Hubbard model. What was written for the average order is also valid here: The values are trustable up to 5.5.

to 5 the distribution only broadens a little bit. At around $t_{exp} = 5.5$ there are configurations with larger n and at around $t_{exp} \approx 6$ the deviation from the initial distribution is clearly visible. Figure 7 shows that as the distribution of the configuration length gets out of hand, the physical observables remain stable despite the anomalies of the distribution. Having explained our findings for the one-site model at large times we can compare Monte-Carlo observables for chains of different length. In figure 8 we show the dependence of the average configuration length on the chosen t_{exp} for different chains. We find that $\bar{n}$ increases linearly with t_{exp}, which is in agreement with findings of [18], and extends them to the case of the combined imaginary-time and real-time approach we use. In the logarithmic plot of figure 9 we see the decay of the average sign depending on the chosen t_{exp}. We see that it decays roughly exponentially for all examined system sizes. We conclude from Figure 8, that the linear increase of the perturbation order with t_{exp} is not a very severe problem. The real limiting factor is, as shown in figure 14, the dynamical sign problem arising from the different sources of imaginary units in the expansion of the observables (see eq. (4.31)), like the complex-valued free Green's function and the

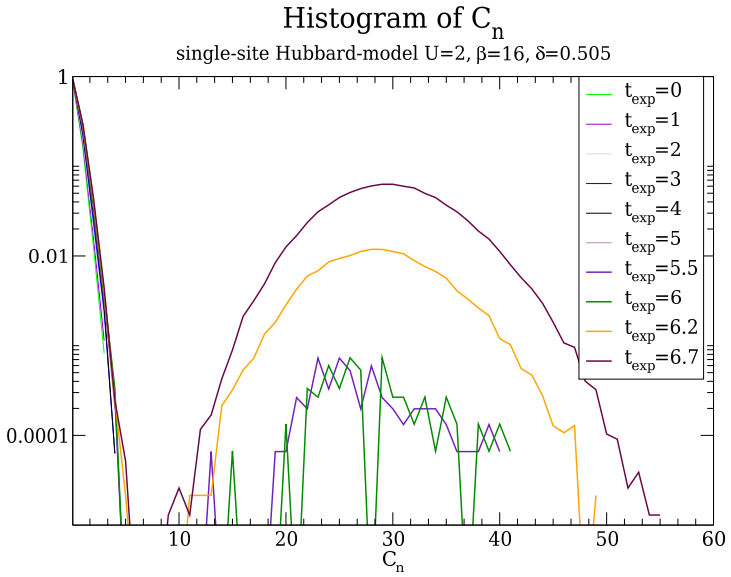

Figure 6: A plot of the distributions of $\log(C_n)$ at different t_{exp}. All distributions are normalized in that way, that $p(C_0) = 1$.

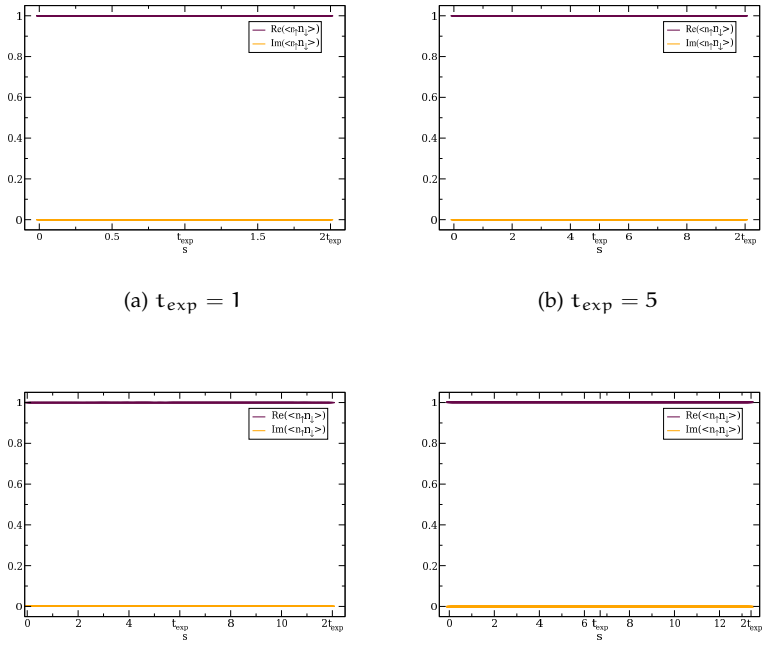

(a) $t_{exp} = 1$ (b) $t_{exp} = 5$

(c) $t_{exp} = 6$ (d) $t_{exp} = 6.7$

Figure 7: The double-occupancy of the single-site Hubbard-model for different times. As predicted they're straight lines. Also for times larger than $t_{exp} = 6$ the observables remain constant albeit the distribution(Figure 6) contains anomalies.

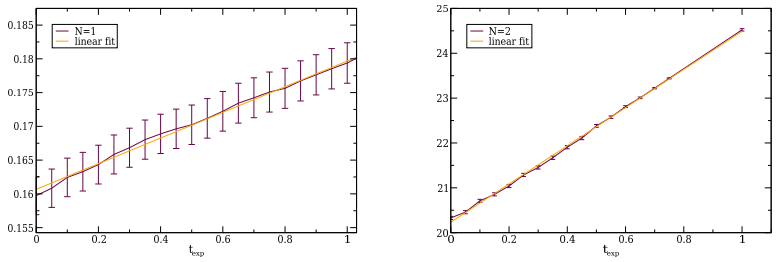

(a) N = 1 (b) N = 2

(c) N = 3 (d) N = 4

Figure 8: Configuration length vs. t_{exp} for chains of different lengths. The linear increase is clearly visible.

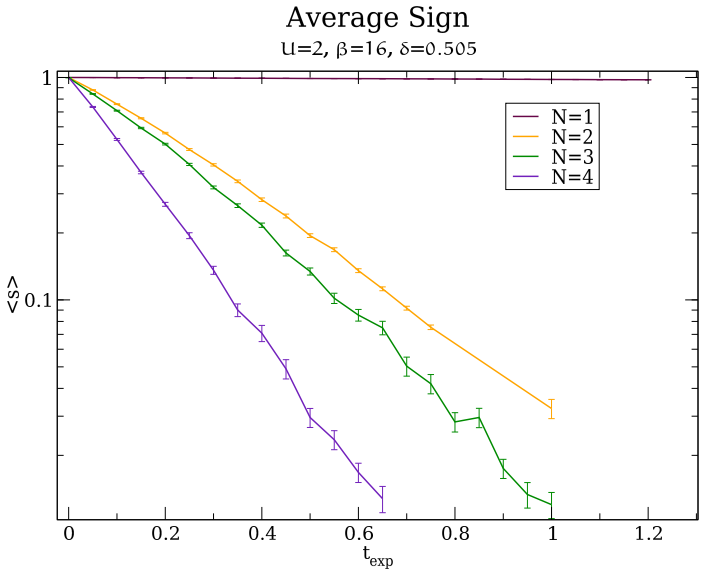

Figure 9: In this logarithmic plot we see the decay of the average sign depending on t_{exp}. It decays roughly exponentially.

phase-factors. For system-sizes up to ≈ 4 we can get a controllable sign to $t_{exp} \approx 1t$(t, the hopping parameter). If we make the usual assumption that t is approximately of the magnitude of $1eV$ this would correspond to $t_{exp} \approx 10^{-15} = 1fs$ in SI-units. As only time-scales of femtoseconds are accessible to us, we are limited to the study of electron dynamics. Figure 10 proves that the Monte-Carlo process is able to reproduce the expected straight lines within the error bars. As examples we have chosen a one-particle observable like the kinetic energy $\langle H_0 \rangle$ and a two-particle observable like the double occupancy $\langle n_\uparrow n_\downarrow \rangle$. These physical observables remain constant for all times independent of the chosen t_{exp}, although increasing t_{exp} worsens the sign-problem and thus leads to bigger error-bars. As Figure 10 also shows the values of the observables are symmetric around their maximum t_{exp} and, being real-valued observables, their imaginary parts vanish within their error-bars. This symmetry around t_{exp} is also seen in the real-time axis part (between 0 and $2t_{exp}$) of the contour-ordered Green's function $G^{\uparrow}_{00}(s,0) = \langle c^{\dagger}_{0\uparrow}(s) c_{0\uparrow} \rangle$. Knowing that the average sign decreases with increasing system size we have chosen the two-site model for the study of further properties of the average sign and its dependence on other parameters. Figure 11 shows the Green's function on the first site of a two-site Hubbard-model. We clearly see the oscillating behaviour on the real-time axis and that G is symmetric at t_{exp}. For $s > 2t_{exp}$ G reduces to an imaginary-time Green's function $G(\tau, 0)$. We also know that for the Hubbard-model the imaginary-time Green's function is a real-valued entity, which is also the case for the contour-ordered Green's function where the imaginary-part vanishes for $s > 2t_{exp}$. In Equation 4.16 we have introduced the parameter δ, of which we claimed that it can be used to reduce the sign-problem. Figure 12 shows the dependence of the average sign on δ. In the particle-hole-symmetric case($N = 2, 4$) the average sign can be improved by lowering δ close to 0. This also leads to a decrease of the average order $\bar{n}$, although one has to take care that a small δ can lead to a suppression of even expansion-orders in the Hubbard-model. Because of this $\delta = 0$ is usually not a good choice. This optimization doesn't work away from particle-hole symmetry($N = 1$ and 3). A value like $\delta = 0.5 + 0^{+}$ is best then [44]. Another interesting question was how the average sign depends on β for a given expansion time. Figure 13 shows that the sign remains approximately constant for $\beta \in [1, 128]$. Choosing a β lower than $t_{exp} \approx 0.5$ leads to an increase from $s \approx 0.2$ to $s \approx 0.3$. Thus if we have a β significantly larger than t_{exp} we are in a regime dominated by the imaginary time and if we are smaller than t_{exp}, where the sign remains at least a bit constant we are in a regime where the real-time evolution is dominant. At last we take a look at the dependence of the system size for some fixed expansion times. Figure 14 shows that the average sign decays very roughly exponentially for a given t_{exp}.

Exciting! isn't it?

$\langle n_\uparrow n_\downarrow \rangle$ and E_{kin} of a two-site Hubbard-model

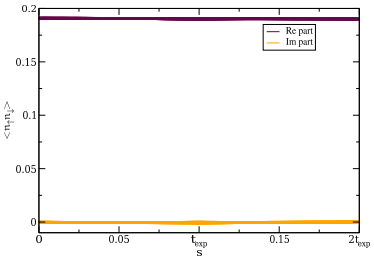

(a) $\langle n_\uparrow n_\downarrow \rangle$ for $N = 2, t_{exp} = 0.1$.

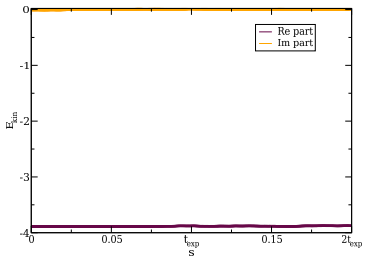

(b) $\langle H_0 \rangle$ for $N = 2, t_{exp} = 0.1$.

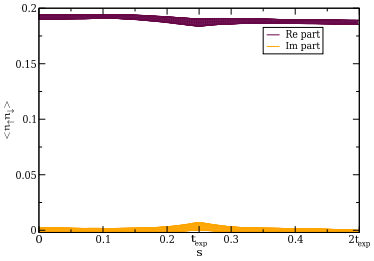

(c) $\langle n_\uparrow n_\downarrow \rangle$ for $N = 2, t_{exp} = 0.25$.

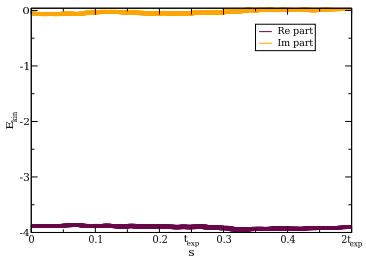

(d) $\langle H_0 \rangle$ for $N = 2, t_{exp} = 0.25$.

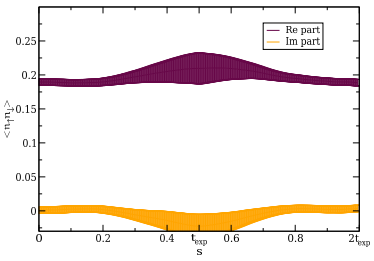

(e) $\langle n_\uparrow n_\downarrow \rangle$ for $N = 2, t_{exp} = 0.5$.

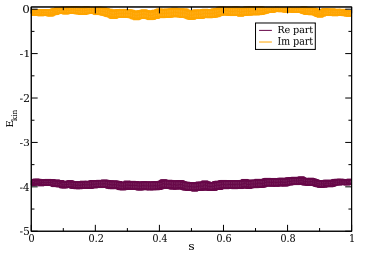

(f) $\langle H_0 \rangle$ for $N = 2, t_{exp} = 0.5$.

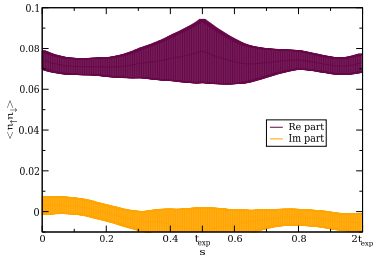

(g) $\langle n_\uparrow n_\downarrow \rangle$ for $N = 3, t_{exp} = 0.5$

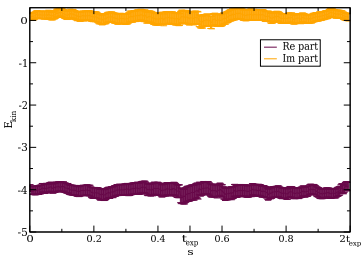

(h) $\langle H_0 \rangle$ for $N = 3, t_{exp} = 0.5$.

Figure 10: The observables remain constant within their error bars. Here $\beta = 16, U = 2, \mu = 0$. We have chosen as an example for a two-particle observable the double-occupancy $\langle n_{\uparrow,0} n_{\downarrow,0} \rangle$ and for a one-particle observable the kinetic energy $\langle H_0 \rangle$.

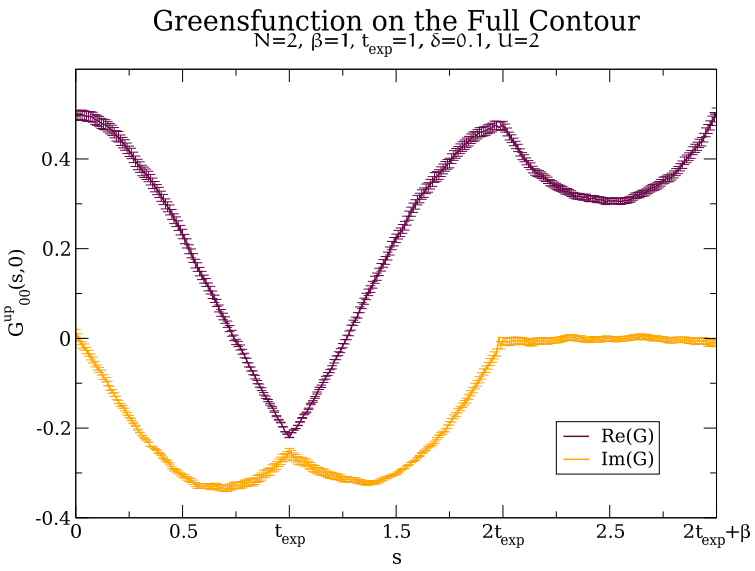

Figure 11: The contour-ordered Green's function $G^{\uparrow}_{00}(s,0)$ of a two-site Hubbard-model along the full interval of s.

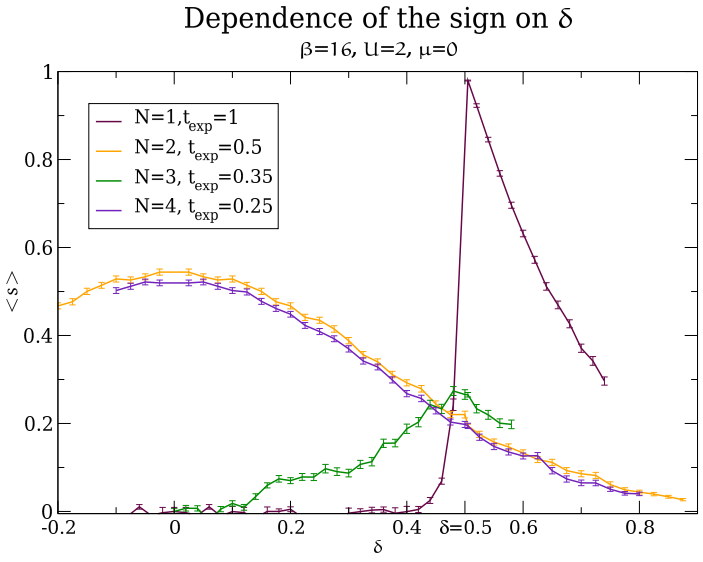

Figure 12: The dependence of the sign on δ.

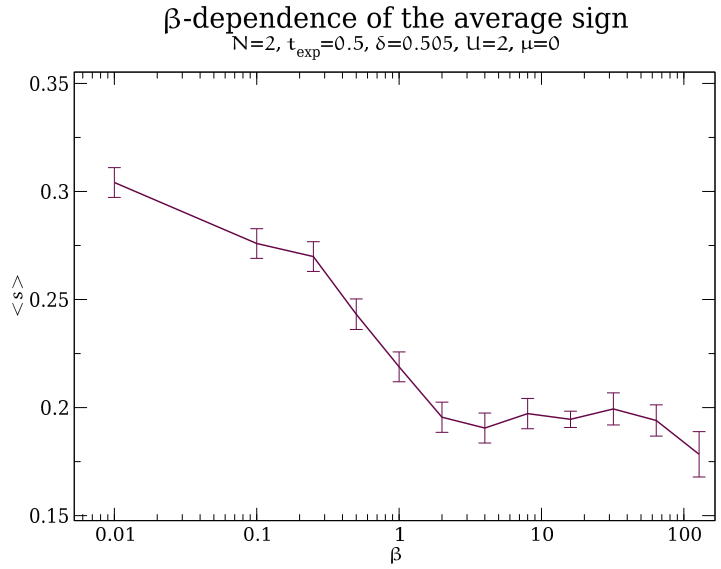

Figure 13: The dependence of the sign on β.

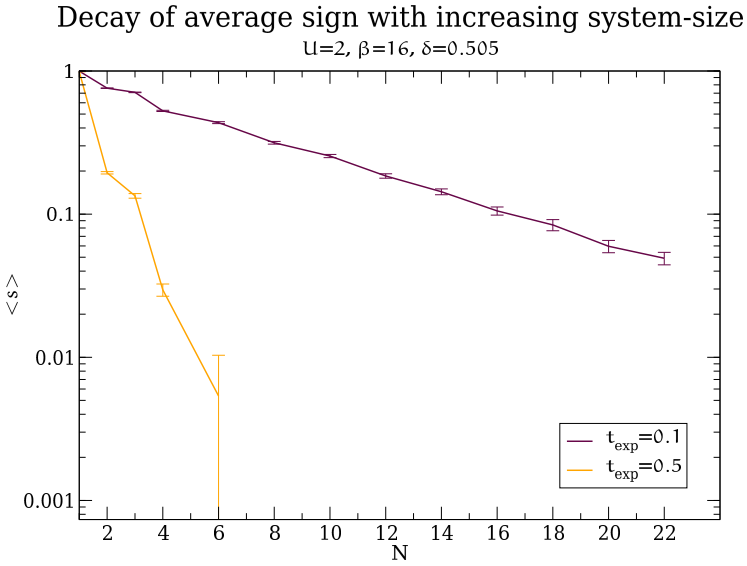

Figure 14: The dependency of the average sign on the system size. It decays roughly exponentially with N.

5.3 KIPPMODELL

Having studied an example without explicit time-dependence the next step was to introduce a time-dependent interaction into the Hamiltonian. There are two possibilities for this, we could introduce a time-dependency into the interaction part and evaluate it with Monte-Carlo or we could introduce the time-dependency into the one-particle part of the Hamiltonian H_0 and hope for an analytic solution of the free Green's function. Now we take a look at the former approach. The "Kipp-Modell" is a two-site Hubbard-model that contains a time-dependent one-particle interaction, and thus allows an analytical calculation of the free Green's function:

$$H = -2t \sum_{\sigma} (c^{\dagger}_{1\sigma} c_{2\sigma} + c^{\dagger}_{2\sigma} c_{1\sigma}) + f(t)(\mu_1 n_1 - \mu_2 n_2) + H_U \quad (5.13)$$

with μ_i being the chemical potential of a site, n_i the number of particles on a site and $f(t)$ is the function for the switching procedure; in our case it is $f(t) = \Theta(t - t_{pert})$. t_{pert} is the time at which the interaction is switched on. The interaction part H_U is the same as in the Hubbard-model and gets evaluated by Monte-Carlo. A bosonic version of a similar model was studied in an experimental setup in [57] with the additional constraint that the chemical potentials are chosen symmetric. They use a setup where they prepared two ^{87}Rb atoms in an optical lattice. Applying a magnetic field, the potential bias between different sites can be changed. On timescales of ms they observe oscillations of the spin population due to super exchange interactions. Lacking access to ms timescales we use the model just as another benchmark to show that the algorithm is able to reproduce true time-dependent behaviour with different initial conditions within the limits set by the sign problem. As the algorithm needs free Green's functions as its input we start by sketching the calculation. The Heisenberg-equation (3.5) for the fermi-operators leads us to consider

$$-i\frac{d}{ds}\begin{pmatrix} c^{\dagger}_{1\sigma} \\ c^{\dagger}_{2\sigma} \end{pmatrix} = \begin{pmatrix} \mu_1 f(s) & 2t \\ 2t & \mu_2 f(s) \end{pmatrix} \begin{pmatrix} c^{\dagger}_{1\sigma} \\ c^{\dagger}_{2\sigma} \end{pmatrix}. \quad (5.14)$$

The equations for the annihilators are the same except for a global minus-sign on the right-hand-side. These Equations have to be solved subject to the initial condition

$$c^{\dagger}_{x}(t_{pert}) = c^{\dagger}_{x}. \quad (5.15)$$

We only go through the calculation of the part where the new chemical potentials act. The time-dependency of the operators on those parts of the contour without chemical potential can be derived by setting μ_1, μ_2 to zero. The eigenvalues of the above equations are

$$\lambda_{1/2} = \frac{\mu_1 - \mu_2}{2} \pm \frac{1}{2} A. \quad (5.16)$$

with $A = \sqrt{(\mu_1 + \mu_2)^2 + 16t^2}$. Thus in its eigensystem the time - dependence of new operators α is

$$\alpha^{\dagger}_{1\sigma}(s) = \alpha^{\dagger}_{1\sigma}(0) e^{i\lambda_1 z(s)} \quad (5.17)$$

$$\alpha^{\dagger}_{2\sigma}(s) = \alpha^{\dagger}_{2\sigma}(0) e^{i\lambda_2 z(s)}. \quad (5.18)$$

In the space of the $c^\dagger$'s this means

$$\begin{pmatrix} c_1^\dagger(s) \\ c_2^\dagger(s) \end{pmatrix} = \frac{1}{N_1} \begin{pmatrix} 2t\alpha_1^\dagger(0)e^{i\lambda_1 z(s)} - x\alpha_2^\dagger(0)e^{i\lambda_2 z(s)} \\ x\alpha_1^\dagger(0)e^{i\lambda_1 z(s)} + 2t\alpha_2^\dagger(0)e^{i\lambda_2 z(s)} \end{pmatrix} \tag{5.19}$$

where we introduced $x = \lambda_1 + \mu_2$ and $N_1^2 = 4t^2 + x^2$. The $\alpha_x^\dagger(0)$'s can be determined from the initial conditions (5.15). A similar calculation for the annihilators gives

$$\begin{pmatrix} c_1(s) \\ c_2(s) \end{pmatrix} = \frac{1}{N_1} \begin{pmatrix} 2t\alpha_1(0)e^{-i\lambda_1 z(s)} - x\alpha_2(0)e^{-i\lambda_2 z(s)} \\ x\alpha_1(0)e^{-i\lambda_1 z(s)} + 2t\alpha_2(0)e^{-i\lambda_2 z(s)} \end{pmatrix} \tag{5.20}$$

with similar initial conditions. Having the evolution of the Fermi-operators one can start piecing together the lesser and greater Green's functions like $G_{ij}^{0,>}(s,s') = \langle c_i^\dagger(s)c_j(s')\rangle$ and vice-versa for $G^{0,<}(s,s')$. Having introduced a true time-dependency we can start to compare our results to more interesting functions than straight lines. The exact results were derived using ED with Mathematica. Figure 15 shows that a one-particle observable like the Kinetic Energy can be reproduced. Figure 16 shows the same for a two-particle-observable like the double-occupancy. In figure 17 we compare the kinetic energy with different initial conditions. We see that if the perturbation sets in at a later time t_{pert} the behaviour of the kinetic energy afterwards is reproduced and that up to that point the thermodynamic value is reproduced within its error bars. Thus we conclude that the algorithm is able to reproduce time-dependent behaviour in simple models.

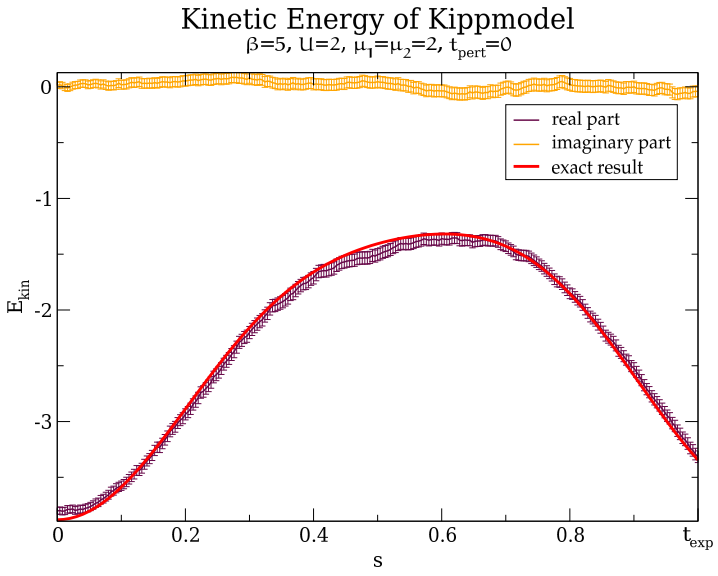

Figure 15: We compare the Kinetic Energy to exact results.

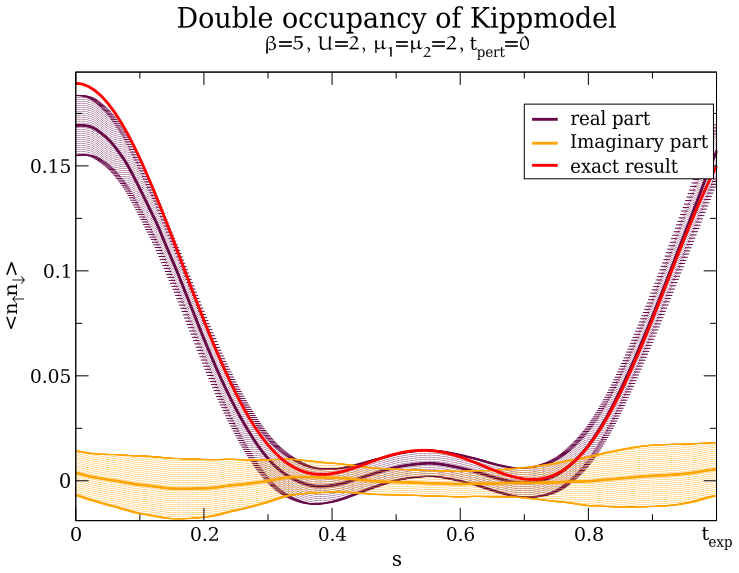

Figure 16: We compare the double occupancy to exact results. The shaded area around the thicker lines is the area that is taken up by the error-bars.

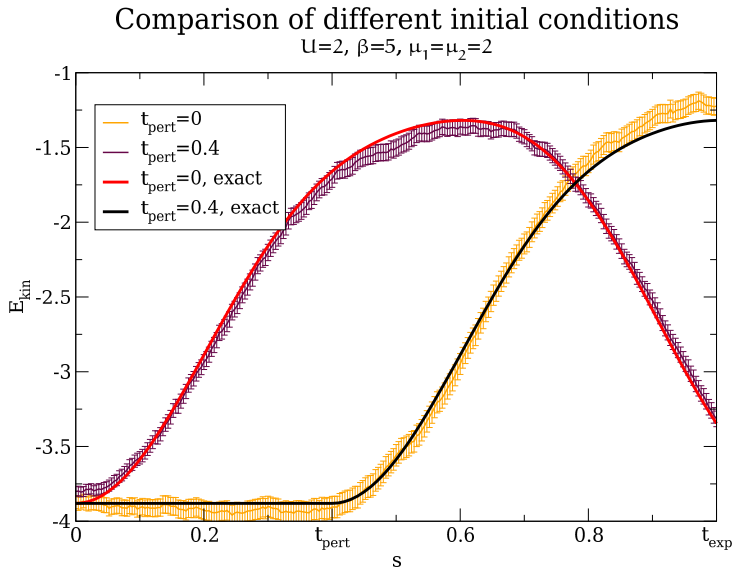

Figure 17: We compare the Kinetic Energy at different initial conditions

6

AN EXAMPLE FROM ULTRACOLD-ATOM EXPERIMENTS

I love deadlines.
I like the whooshing sound they make as they fly by.

— Douglas Adams

6.1 INTRODUCTION

Ultracold quantum gases received much attention lately from theoretical physicists due to the possibility to study many-particle models ,not in some "dirty" environment like solid states where the models always present some kind of idealization, but very much like in a clean laboratory. Besides the realization of phenomena that are already known from real world solid state physics it is also interesting to ask whether the new degrees of freedom offered by cold atom experiments could give rise to states of matter which do not have obvious counterparts in the known interacting electron physics. In this vein [59] explored the dependence of the 2D $SU(N)$ Hubbard-model and thus its dependence on the number of internal symmetries with an functional Renormalization Group (fRG)-method in anticipation of a future realization in cold atom experiments. The new opportunities that experiments with ultracold atoms offered sparked a lot of research into the nonequilibrium dynamics of the Hubbard-model. In this context we study the effect of the rapid change of a parameter of a physical model. We consider a 1D Hubbard-model where the Hubbard-interaction H_U is switched off at time 0.

Despite mainly being a zoological garden for theoretical physicists there might be applications for ultracold quantum gases as sensitive devices for force measurements [58].

$$H(t) = H_0 + (1 - \Theta(t))H_U \tag{6.1}$$

Note that we neglected the interaction with an optical trap. Thus we have prepared the system in a correlated initial state given by $H_0 + H_U$ and evolve the system only with H_0. Due to this particular real-time dynamics a number of questions arise:

- Does the system evolve to a new steady-state?
- What is the nature of this state?
- Does the system retain memory of the initial state?
- Is the new state related to the initial thermal equilibrium state?

Some of these questions have been addressed for similar models in the literature There has been extensive work on 1D bosonic systems experimentally [36, 60] as well as theoretically [61, 62, 63] for nearly integrable systems. [60] investigated the thermalization of strongly interacting ultracold atoms in a nearly integrable situation and found that on the experimentally accessible time-scales the thermalization to the initial state

did not occur but instead to a non-thermal steady state was reached. The transition from a metallic to an insulating state of the 3D fermionic Hubbard model depending on the confinement was studied in [64]. 1D Fermionic models in an optical trap at $T = 0$ were treated numerically in [65]. They found Mott-insulating regions in certain ranges of U and the total particle number N. In the experiments where thermalization to a non-thermal steady-state was observed, the existence of the different steady-state has been linked to the integrability of the examined systems, which inhibits the full relaxation due to additional conserved integrals of motion. But as the numerics showed even detuning the models away from integrability did not always lead to the thermal steady state, but often the systems did not equilibrate. In the classical case it is assumed that non-linearities in the equations of motion generate chaotic behaviour and will finally lead to the thermalization of the system. This behaviour is not present in quantum mechanics where the unitary time-evolution operator $U(t, t_0)$ acts on an initial state from the Hilbert-space in a way such that the initial state is mapped on a time-parametrized trajectory of states where the constraints given by the integrals of motion always hold. Expectation-values of observables also show the equilibration to non-thermal equilibrium states. To account for the behaviour in integrable systems it was suggested that generalized statistical ensembles that explicitly contain the conserved quantities can be used to describe the long-term stationary behaviour[66], similarly to the construction of statistical mechanics from the principle of Maximum Entropy constrained by the conserved quantities [67, 68]. But that still leaves open the question why non-integrable systems can exhibit a thermal long-time behaviour and for what reason. In earlier works a possible solution to this dilemma was the proposed ETH by Deutsch[69] and Srednicki[70] which was also invoked to explain recent numerical results [71]. The ETH states that given the expectation value $\langle\Psi_\alpha|A|\Psi_\alpha\rangle$ of a few-body observable A in an eigenstate $|\Psi_\alpha\rangle$ with energy E_α, of a large interacting many-body system equals the thermal, microcanonical average $\langle A\rangle_{\text{micro}}(E_\alpha)$ of A at the mean energy E_α:

$$\langle\Psi_\alpha|A|\Psi_\alpha\rangle = \langle A\rangle(E_\alpha) \tag{6.2}$$

What does this mean for the emergence of the final thermal state? This means that every eigenstate of a Hamiltonian always implicitly contains a thermal state. Initially the coherence between the states hides the thermal state, but dephasing due to time dynamics reveals it (Figure 18). There are no definite general proofs for the validity of ETH but there are results in some limits and a number of numerical results(see [71, 61, 72]). A similar model as ours without interactions was studied using a QMC-solver within the DMFT framework in [35] with the difference that instead of starting from a correlated initial state they started from free electrons and switched on U at $t = 0$. They studied the resulting dynamics due to the quench from small U values to large U values and found that a rapid thermalization occurs at large and small values of U and that at a critical $U_c^{dyn} = 3.2$ the oscillations fade out. They call this a *dynamical* phase transition. It is not clear whether there is a relation to a thermodynamic phase-transition.

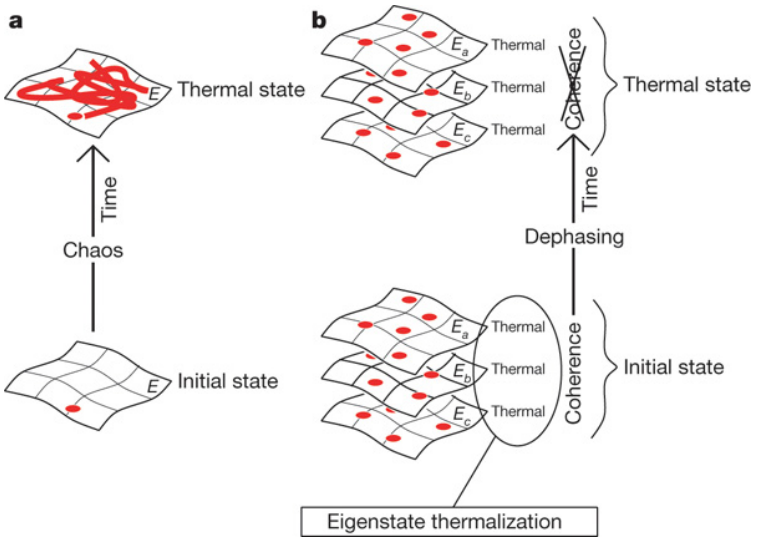

Figure 18: Thermalization in classical vs. quantum mechanics. From [71]

6.2 OBSERVATIONS

In our simulation we start from a finite U and release the system to $U = 0$, so we just have to prevent the Monte-Carlo process from generating interaction-vertices on the real-time axis. *Because of this and because we're in 1D we don't suffer from the sign problem and have the possibility to access arbitrarily large times.* Of course we first had to benchmark this approach, so we compared to ED data[73]. We can see

Comparison with Data from ED

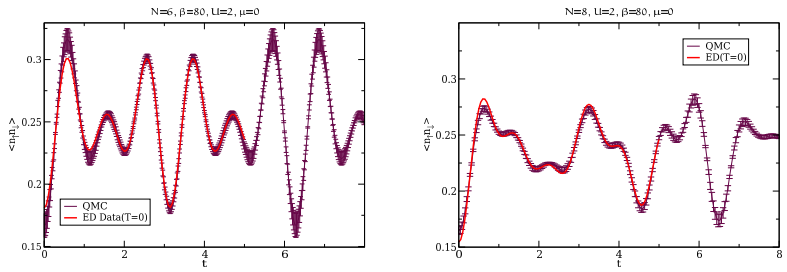

(a) $N = 6$ (b) $N = 8$

Figure 19: We compare the double occupancy from the simulation to some data from ED.

that the code that implements the algorithm handles that case rather well. We can already deduce from the results produced so far, that we expect most observables to oscillate to some new behaviour and that we might need larger system sizes to get a grip of the finite size effects. Next we compare some correlation functions to the naive expectation that the system should relax to a state given by the pure non-interacting density matrix $\rho_0 = e^{-\beta H_0}$. Values determined with this density-matrix are given by the red thick lines in the diagrams.

6.2.1 *Charge-charge correlation functions*

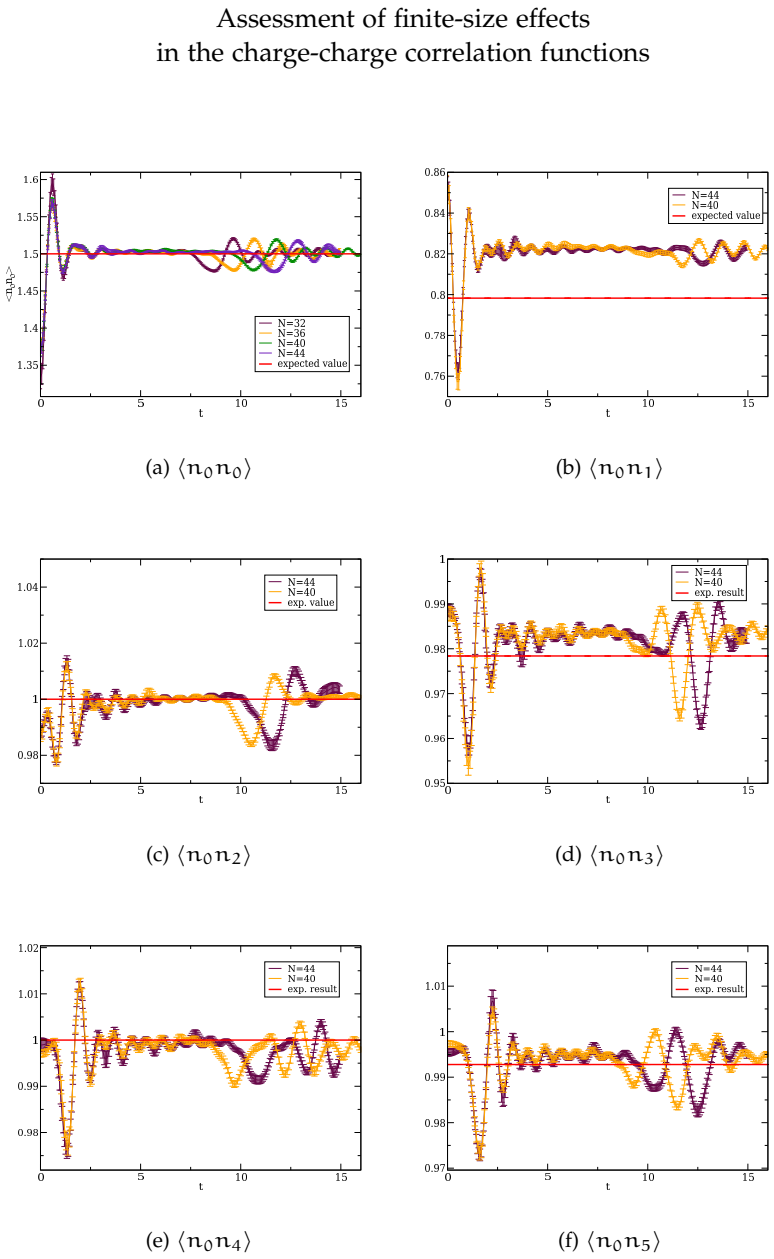

(a) $\langle n_0 n_0 \rangle$ (b) $\langle n_0 n_1 \rangle$

(c) $\langle n_0 n_2 \rangle$ (d) $\langle n_0 n_3 \rangle$

(e) $\langle n_0 n_4 \rangle$ (f) $\langle n_0 n_5 \rangle$

Figure 20: Charge-charge correlation functions for sites of different distances. We compare chains of length 44 with shorter chains to check for finite-size effects. Here $\beta = 15, U = 2, \mu = 0$.

Figure 20 shows the Charge-Charge-correlation function of site 0 with sites 0 to 5. We don't show longer correlations as their values are too early limited by finite-size effects. The charge-charge-correlation-function between different sites is defined as

$$\langle n_i n_j \rangle = \langle (n_{i,\uparrow} + n_{i,\downarrow})(n_{j,\uparrow} + n_{j,\downarrow}) \rangle. \tag{6.3}$$

Note that in this correlation function the uncorrelated part $\langle n_i \rangle \langle n_j \rangle = 1$ is still included. The correlation function in figure 20a allows us to observe the finite size effects. The dependence of the first reoccurring oscillation is linear in the system size. Thus the finite-size effects limit

the maximum time for which we can do meaningful measurements, and the linear dependence might be expected for a 1D system. We see that after some initial oscillations the correlation functions reach a new steady state. There seems to be some kind of odd-even effect at work here as the new steady state of even distance correlation functions is the thermal one of ρ_0, whereas the new state reached by the odd distances is not the expected state. This might be due to the anti-ferromagnetic ordering present in the ground-state of the 1D Hubbard-model. That the reached values don't necessarily match the values determined with ρ_0 is no surprise, because — as stated before — the additional conserved quantities should be taken into account when trying to construct a new density-matrix that describes this new state. As one increases the distance in the even case the reached state more closely resembles the expected value(assuming that the clearly visible finite size effects play no role).

6.2.2 *Spin-spin correlation functions*

Next we are looking at spin-spin correlation functions. The spin-spin correlation function is defined as

$$\langle S_i^z S_j^z \rangle = \frac{1}{4} \langle (n_{i,\uparrow} - n_{i,\downarrow})(n_{j,\uparrow} - n_{j,\downarrow}) \rangle \tag{6.4}$$

with the familiar S^z operators, where it is implicit that we chose z as the quantization axis. This is the pure correlated part as $\langle n_{i,\sigma} \rangle - \langle n_{j,\sigma} \rangle = 0$. We see similar structures like in the charge-charge-correlation functions.

Spin-spin correlation functions

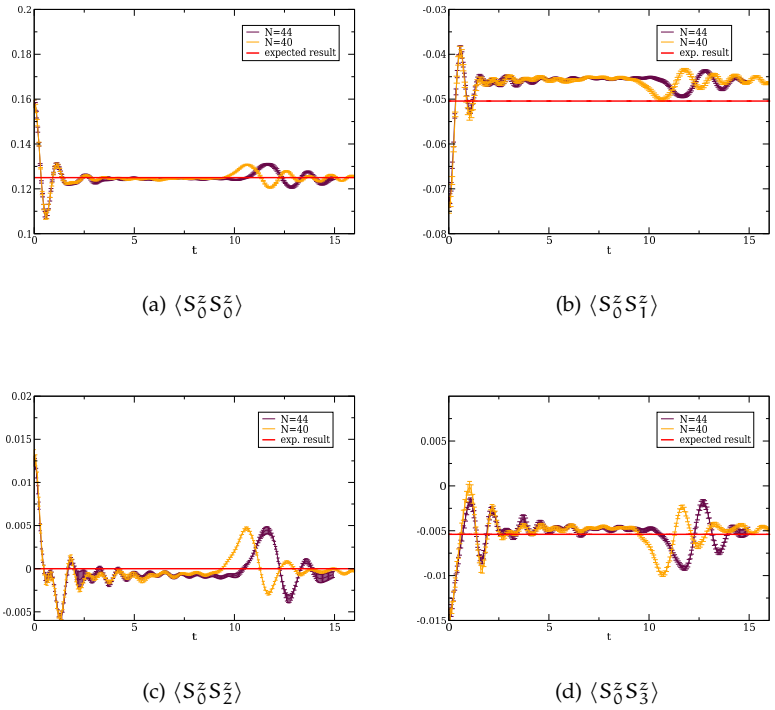

(a) $\langle S_0^z S_0^z \rangle$ (b) $\langle S_0^z S_1^z \rangle$

(c) $\langle S_0^z S_2^z \rangle$ (d) $\langle S_0^z S_3^z \rangle$

Figure 21: Spin-spin correlation functions for sites of different distances We compare lattices of length 44 with lattices of length 40 to check for finite-size effects. Here $\beta = 15, U = 2, \mu = 0$.

The finite-size effects limit the maximum time that we can observe to around 10 in the case of the 44-site chain. The correlation on the same site (figure 21a) decays rather fast and shows almost no oscillations, but as we increase the distance the oscillations remain longer and from a distance of 3 onwards we're probably limited by finite-size effects and can't see the reaching of a new steady state. Except probably the on-site correlation, no spin-spin-correlation function equilibrates to the value given by ρ_0.

As a lot of spin-spin correlations are close around a value of 0 it is interesting to take a look at the correlations in k-space. The correlation

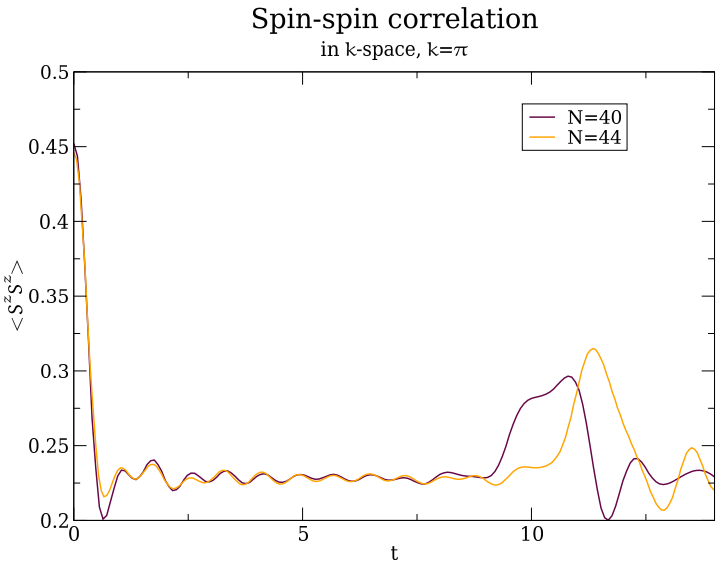

Figure 22: Spin-spin correlation for $k = \pi$. No error bars are available.

between spins moving in different directions decays very fast(the minimum of the first drop is around $t = 0.65$) and then oscillations around a value of $S(\pi, t = 0)/2$ arise. Due to the lacking error bars there's probably no right way to assess the finite-size effects, but judging from the second reoccurring oscillation at $t \approx 9$ to $t \approx 10$(that distinguishes the two graphs quite a bit), we can guess that we're seeing the steady state behaviour up to ≈ 9. This is a clear indicator of a memory-effect. In comparison the spin-spin correlations of a free electron-gas, as given by ρ_0, vanishes. But in our case they remain clearly visible as their numerical value only halves.

6.2.3 η-*pairing correlations*

There's one interesting observable left in the data from our simulations: the η-pairing. An η-pair is created by

$$\eta_Q^\dagger = \sum_k c_{k,\uparrow}^\dagger c_{-k+Q,\downarrow}^\dagger. \tag{6.5}$$

We define the η-pairing correlation function as:

$$\langle \eta_Q^\dagger(t)\eta_Q(t)\rangle = \sum_{k,k'} \langle c_{k,\uparrow}^\dagger(t) c_{-k+Q,\downarrow}^\dagger(t) c_{-k'+Q,\downarrow} c_{k',\uparrow}\rangle. \tag{6.6}$$

Interestingly the η-pairing provides an additional conserved quantity if the chain has an even length. As the evolution of a creation-operator is given by $c^\dagger_{k,\sigma}(t) = e^{-it\epsilon(k)}c^\dagger_{k,\sigma}$, an η-pair evolves like

$$\eta^\dagger_Q(t) = \sum_k e^{it(\epsilon(k)+\epsilon(-k+Q))}c^\dagger_{k\uparrow}c^\dagger_{-k+Q,\downarrow} \tag{6.7}$$

with $\epsilon(k) = -2t\cos(k)$. This quantity is a constant of motion if $Q = \pi$. This can be observed for example in Figure 23 as the value given by $n = 22$. Comparing with the lattice of length 40 (η-pairing not shown)

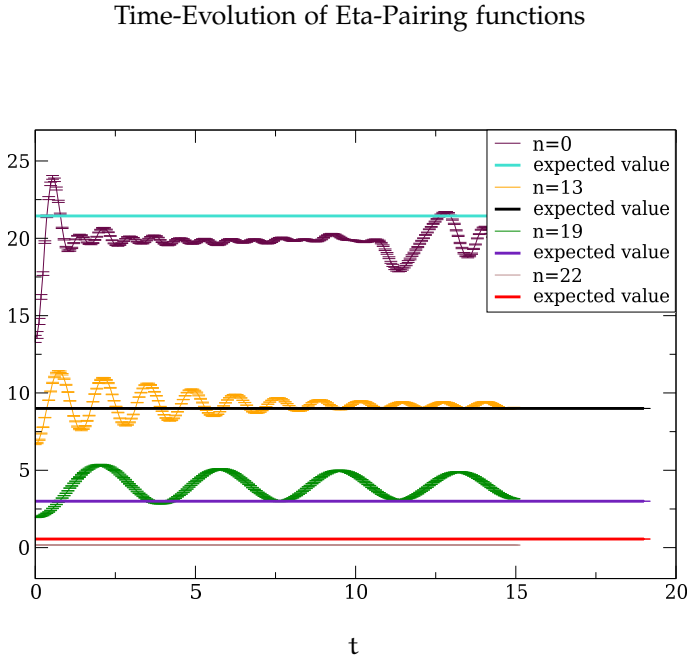

Figure 23: The η-pairing. The values of n that are given in the legend determine the impulse as $Q = \frac{2\pi n}{N}$. For a given value of n the color directly below in the legend shows the value determined with ρ_0. Here $\beta = 15, U = 2, \mu = 0, N = 44$.

we can deduce that the finite-size effects are Q-dependent. For the $Q = 0$ correlation the finite-size effects limit the time to ≈ 11.6. But this seems to be sufficient to probably observe steady-state behaviour in a non-thermal state as the graph is a large way off the expected value. As we go to higher values the finite-size effects are not visible and the period of the oscillations get longer. Also no correlation function reaches the values determined with ρ_0. In particular the particle-hole symmetric point $Q = \pi$ is constant (that's expected, we've proven that it's a constant of motion) but is visibly away from the value determined with ρ_0.

We've seen that a lot of observables that we studied didn't equilibrate to a steady state given by the density-matrix ρ_0, as one might expect in a first, naive guess. The construction of a density-matrix that describes this new steady state should take into account the constraints given by the additional conserved quantities. Additional conserved quantities are all particle-densities in k-space because

$$[H_0, n_{k,\sigma}] = 0.$$

As $n_{k,\sigma}$ is a conserved quantity the fermi-surface of the initial system, given by ρ, stays conserved for the whole time-evolution. Another conserved quantity is the particle-hole symmetric point with $Q = \pi$ of the η-pairing.

Future work that tries to construct the density-matrix of the non-thermal steady-state would thus have to take into account at least the particle-densities $n_{k,\sigma}$ and the particle-hole symmetric point of the η-pairing. Since in [35] the existence of a prethermalization regime is mentioned we should check with larger times to make sure that a thermalization doesn't occur after longer times.

6.2.4 *The dynamics of the transition from the Mott-insulator to a metal*

Having studied the time-evolution of some observables we take a look at the evolution of the lattice as a whole. First we look at the correlated part of the charge-charge correlation, that is $\langle n_i n_j \rangle - 1$. Figure 24 shows the evolution of the charge-charge correlation function in the lattice for different times. For $t = 0$ we see signatures of the exponential decay of the correlation with the distance — a characteristic of an insulating state, here due to the Mott-insulating state of the Hubbard-model. Later for $t = 1.2$ we see the emergence of a front from left with approximately constant correlation. This is a signature of the metallic state that is beginning to propagate through the lattice. To the right of the front the exponential decay is still present and thus there still is the insulating state. At later times the front propagates further through the lattice up to a time of around $t = 4.2$ where we're limited again due to finite-size effects as the front comes from is meeting its partner that propagated to the right. For $t = 3.0$ the front has approximately reached site 13 thus it has velocity $v_C = 13/3.0 \approx 4.3$, that is it propagates 4.3 sites for a interval of time of 1. This little argument is in nice agreement with an analysis by linear regression which yields a velocity of the change in the charge-charge correlation of $v_C = 4.14 \pm 0.17$. The emergence of that front in the charge-charge correlations is in agreement with mean-field calculations [73]. Thus we observe the expansion of a metallic state through the lattice. Notable, but expected, is the dependence of the speed on the remaining parameter t of the model. Thus the system is not immediately transforming to a metallic state but only as fast as the front propagates through the system and the speed is given by a model parameter.

The most visible effect of this subtraction is the explosion of the error bars...

Periodic boundary conditions!

There is also a front in the pairing correlation functions, as shown in Figure 25, although a little more goodwill and guesswork are needed. For $t = 0$ we see the initial state of the Hubbard-model, something like an exponential decay from which we conclude that the system is an insulator for the transport of η-pairs. At $t = 0.6$ we can guess the development of a front and still see the exponential decay to the right of it. At $t = 1.8$ the front on the left side of the picture is clearly visible and the exponential decay to the right of it can be guessed. For $t = 3.6$ we are again limited by the finite size effects but we see that large parts of the system have chosen to get into the plateau part of the front which should allow the transport of η pairs. The emergence of the front in the η-pairing is consistent with meanfield calculations [73]. We can also determine the speed of the front for the η-pairing. Linear regression gives for the velocity of the change in the η-pairing of $v_\eta = 4.69 \pm 0.21$ which is a bit faster than the velocity of the charge. But they would be consistent within two standard deviations.

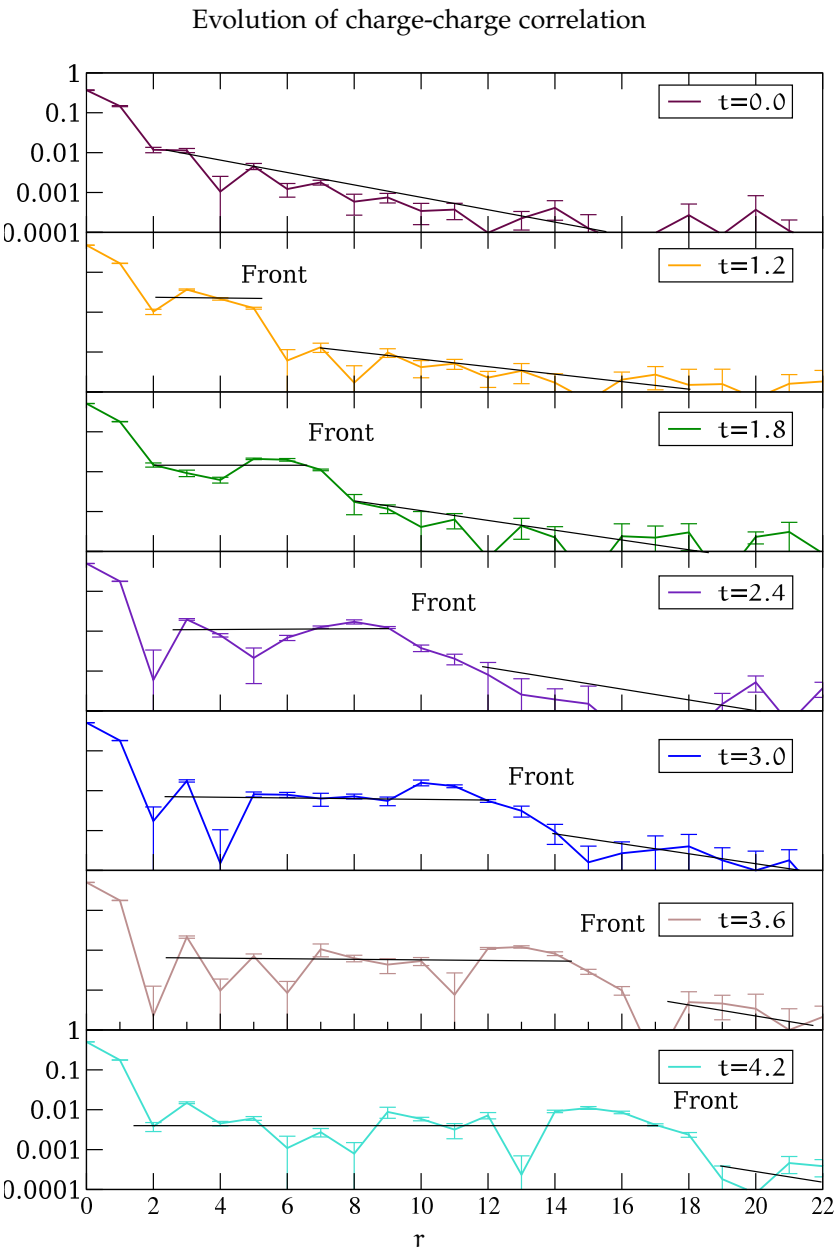

Figure 24: The transition from the insulating state of the Hubbard-model to something that more resembles a metal as seen in the charge-charge correlation $\langle n_r n_0 \rangle - 1$. For visibility only the first and the last picture have y-axis labels. The x and y scales are the same in all pictures. The black lines are guides for the eye that delineate metallic phases(usually on the left if visible) from insulating phases.

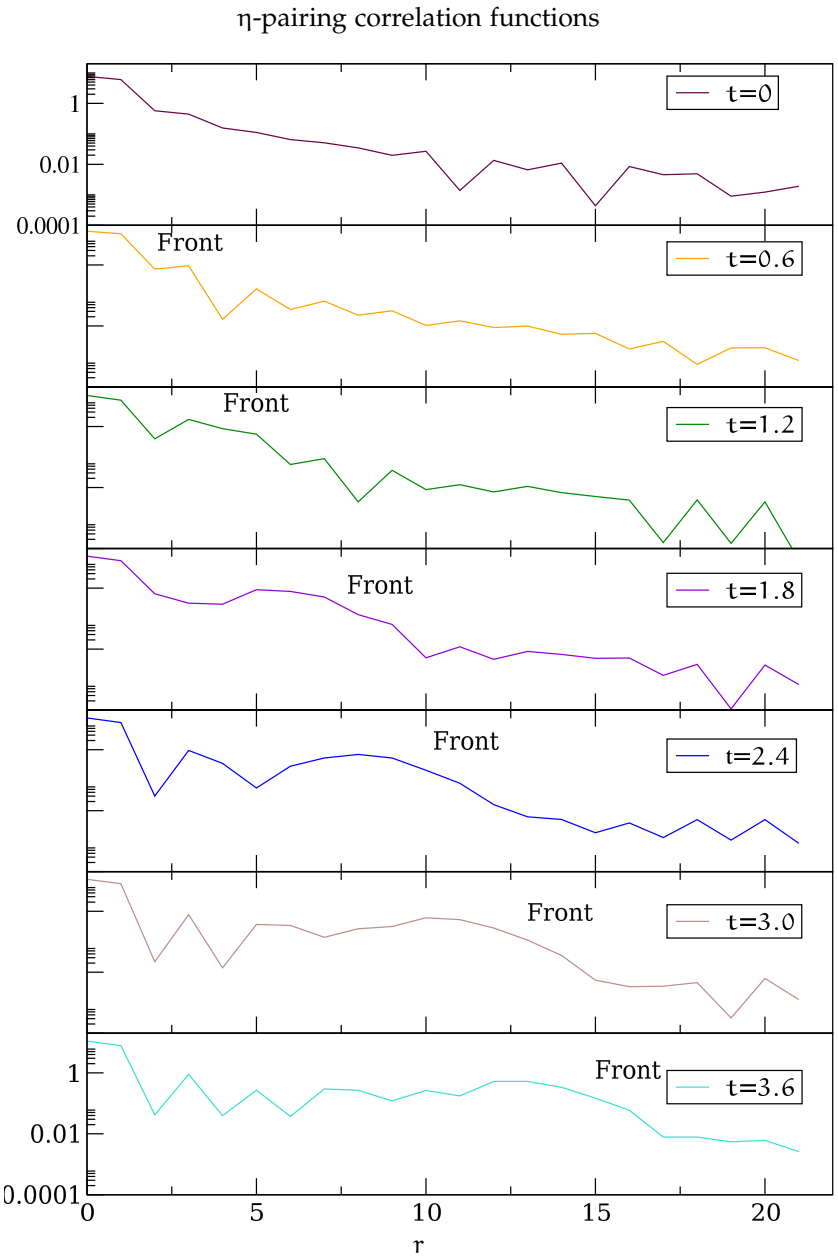

Figure 25: The same transition as in the charge-charge correlation function (24) in the η-pairing $\langle \eta_r \eta_0 \rangle$. For visibility only the first and the last picture have y-axis labels. The x and y scales are the same in all pictures. No error-bars are available but, as a rough guess, they should resemble those of figure 24.

The same study in the spin-spin correlation function through the whole lattice proceeds a bit differently. Figure 26 shows the spin-spin correlation function for different times across the whole relevant part of the lattice. For $t = 0$ we see the anti-ferromagnetic order of the Hubbard-model. Then, when we switch off U, wait a little bit, and already for $t = 0.42$ the correlations have significantly decreased(see also Figure 27). Waiting till $t = 0.9$ the correlations have completely melted away.

Spin-spin correlation functions for different times

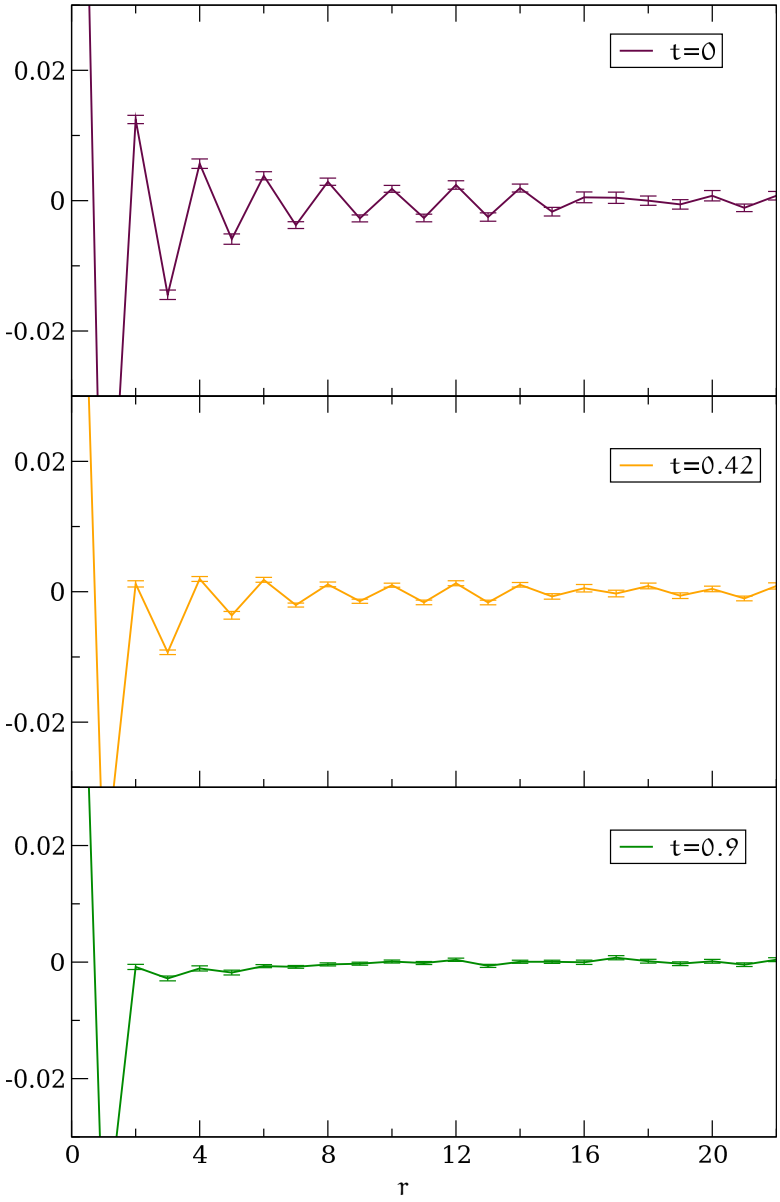

Figure 26: The Spin-spin correlation function $\langle S^z_r S^z_0 \rangle(t)$ for different values of t. The x and y scales are the same and linear in all pictures.

To better observe this change from the initial thermal state we plotted the quantity $\langle S^z_r S^z_0 \rangle(t) - \langle S^z_r S^z_0 \rangle(0)$ in figure 27. For $t = 0.06$ we see that the changes in the correlation have already propagated to the first site. The next picture, 0.06 later, the front of the correlation is two sites

Change of the spin-spin correlation functions depending on time

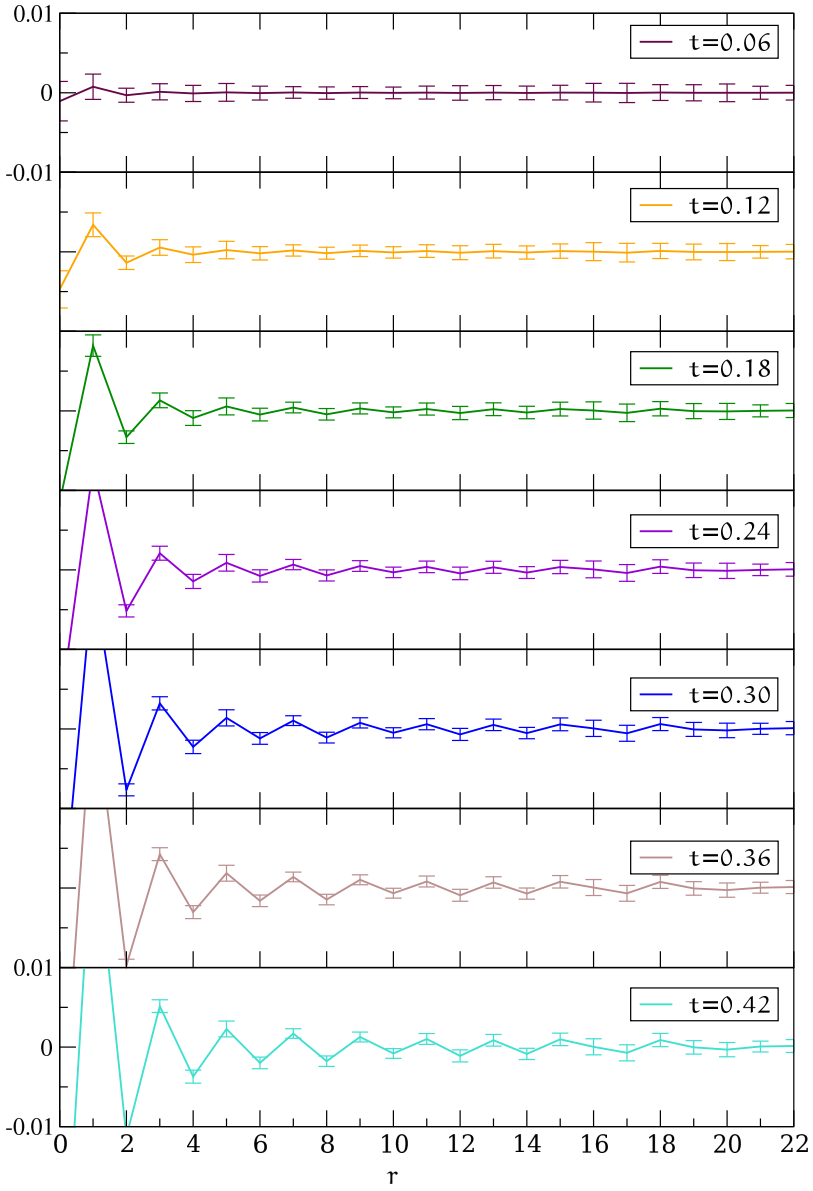

Figure 27: The quantity $\langle S_r^z S_0^z \rangle(t) - \langle S_r^z S_0^z \rangle(0)$. For visibility only the first and the last picture have y-axis labels. The x and y scales are the same in all pictures.

further. It is safe to say that this front has fully traversed the lattice for $t = 0.42$. Thus we see that changes in the spin-structure propagate at least an order of magnitude faster. Linear regression determines the speed of the changes in the spin to $v_S = 59.5 \pm 2.5$. A plot with a logarithmic y-axis scale of Figure 27 would probably provide interesting insights into the behaviour of the system but due to the already large error-bars in the linear plot, we could deduce anything we wanted from it.

Thus we observe different speeds for the transport of changes in the spin structure and for the transport of charge, that resembles a bit the spin-charge separation known form the Luttinger liquid.

7 CONCLUSION

When in doubt, use brute force.

— Ken Thompson

"If brute force doesn't solve your problems,
then you aren't using enough."

Starting from the recently developed DDQMC method we developed a QMC method that allows to study the real-time dynamics of arbitrarily correlated initial states using a joint expansion in imaginary time as well as in real-time. We tested the approach with some simple Hubbard-like toy models where we assessed new effects of the real-time expansion as well as the decay of the average sign. The method seems to be working up to times of about $1t$ (t is the hopping-parameter of the Hubbard-model), due to the constraints given by the dynamical sign problem. As a non-trivial example we studied 1D Hubbard-chains where at time $t = 0$ the interaction term H_U is switched off. We studied the relaxation of the system to a possibly new non-thermal steady-state. We did examine the propagation of the change of the Hamiltonian through the lattice and found that the system seems to evolve to a metallic state. Spin and charge information propagate through the lattice with speeds that differ by about one order of magnitude. As the measurements of the speeds are at the limit of what we can deduce from our data future challenges will include a parallelization of the code to use the power of computer clusters as well as supercomputers to reduce the error bars. As the only source of the speed differences can be in the initial Hamiltonian, a systematic study of the dependence of the speeds on U is in order. Another challenge is the construction of the initial density matrix. To that end we'll have to do simulations with larger system sizes to determine what is really steady-state behavior and to make sure that we don't see a prethermalization regime as mentioned in [35] where observables reached their thermal behavior on very long timescales.

Part IV

APPENDIX

A

FERMION COHERENT STATES

In this section we list some properties and used notations of fermionic coherent states integrals. For other properties and rigorous proofs see [38]. The Unity for the j-th time-slices is

$$\begin{aligned}\mathbb{1}_j &= \int \prod_\alpha d\overline{\phi}_{j,\alpha} d\phi_{j,\alpha} e^{-\overline{\phi}_{j,\alpha}\phi_{j,\alpha}} |\phi_{j,\alpha}\rangle\langle\phi_{j,\alpha}| \\ &= \int d\vec{\overline{\phi}}_j d\vec{\phi}_j e^{-\vec{\overline{\phi}}_j \vec{\phi}_j} |\vec{\phi}_j\rangle\langle\vec{\phi}_j| \\ &= \int d\bar{j} dj e^{-\bar{j}j} |j\rangle\langle j|\end{aligned} \tag{A.1}$$

with $\phi_{j,\alpha}$ being a Grassmann number. The last line is something of a shorthand notation. There's also an expression for the trace operation in coherent states:

$$\begin{aligned}\mathrm{Tr}A &= \int \prod_\alpha d\overline{\phi}_{j,\alpha} d\phi_{j,\alpha} e^{-\overline{\phi}_{j,\alpha}\phi_{j,\alpha}} \langle -\phi_{j,\alpha}|A|\phi_{j,\alpha}\rangle \\ &= \int d\vec{\overline{\phi}}_j d\vec{\phi}_j e^{-\vec{\overline{\phi}}_j \vec{\phi}_j} \langle -\vec{\phi}_j|A|\vec{\phi}_j\rangle \\ &= \int d\bar{j} dj e^{-\bar{j}j} \langle -j|A|j\rangle.\end{aligned} \tag{A.2}$$

BIBLIOGRAPHY

[1] A. de Saint-Exupéry, *The little prince*. (Cited on page 1.)

[2] W. Nolting, *Grundkurs theoretische Physik 7*. Springer-Verlag, Heidelberg, 2002. (Cited on pages 2, 7, 18, 31, and 33.)

[3] J. Schwinger, "Brownian Motion of a Quantum Oscillator," *Journal of Mathematical Physics* **2** (1961) 407–432. (Cited on page 2.)

[4] L. KELDYSH, "DIAGRAM TECHNIQUE FOR NONEQUILIBRIUM PROCESSES," *SOVIET PHYSICS JETP-USSR* **20** (1965) 1018–&. (Cited on page 2.)

[5] S. Fujita, "Resolution of the Hierarchy of Green's Functions for Fermions," *Phys. Rev. A* **4** (Sep, 1971) 1114–1122. (Cited on page 2.)

[6] D. Lee, S. Fujita, and F. Wu, "Effect of Initial Correlation on the Kinetic Equation," *Phys. Rev. A* **2** (Sep, 1970) 854–861. (Cited on page 2.)

[7] A. G. Hall, "Non-equilibrium Green functions: generalized Wick's theorem and diagrammatic perturbation with initial correlations," *Journal of Physics A: Mathematical and General* **8** (1975) 214–225. (Cited on page 2.)

[8] P. Danielewicz, "Quantum Theory of Nonequilibrium Processes, 1," *Annals of Physics* **152** (1984) 239–304. (Cited on pages 2, 9, and 16.)

[9] M. Wagner, "Expansions of nonequilibrium Green's functions," *Phys. Rev. B* **44** (Sep, 1991) 6104–6117. (Cited on pages 2, 11, 12, and 16.)

[10] A. Kamenev, "Many-Body theory of Non-equilibrium systems," `cond-mat/0412296v2`. (Cited on pages 2 and 13.)

[11] A. Kamenev and A. Andreev, "Electron-electron interactions in disordered metals: Keldysh formalism," *Phys. Rev. B* **60** (Jul, 1999) 2218–2238. (Cited on page 2.)

[12] C. Chamon, A. W. W. Ludwig, and C. Nayak, "Schwinger-Keldysh approach to disordered and interacting electron systems: Derivation of Finkelstein's renormalization-group equations," *Phys. Rev. B* **60** (Jul, 1999) 2239–2254. (Cited on page 2.)

[13] R. van Leeuwen, N. E. Dahlen, G. Stefanucci, C.-O. Almbladh, and U. von Barth, "Introduction to the Keldysh Formalism and Applications to Time-Dependent Density-Functional theory," vol. 706 of *Lecture Notes in Physics*. Springer-Verlag, Heidelberg, 2006. `cond-mat/0506130`. (Cited on pages 2 and 17.)

[14] A. Stan, N. E. Dahlen, and R. van Leeuwen, "Time-propagation of the Kadanoff-Baym equations for inhomogeneneous systems," *J. Chem. Phys.* **130** (2009) , `arXiv:0906.1704v1 [cond-mat]`. (Cited on pages 2 and 18.)

[15] P. Schmidt and H. Monien, "Nonequilibrium dynamical mean-field theory of a strongly correlated system," arXiv:cond-mat/0202046 [cond-mat]. (Cited on page 2.)

[16] J. K. Freericks, V. M. Turkowski, and V. Zlatic, "Nonequilibrium Dynamical Mean-Field Theory," *Physical Review Letters* **97** (2006) 266408. (Cited on page 2.)

[17] M. Schiró and M. Fabrizio, "Real-Time Diagrammatic Monte Carlo for Nonequilibrium Quantum Transport," arXiv:0808.0589v1 [cond-mat]. (Cited on pages 2 and 3.)

[18] P. Werner, T. Oka, and A. J. Millis, "Diagrammatic Monte Carlo simulation of non-equilibrium systems," *PRB* **79** (2009) , 0810.2345v2 [cond-mat]. (Cited on pages 2, 3, and 35.)

[19] N. P. Landsman and C. G. van Weert, "Real- and imaginary-time field theory at finite temperature and density," *Physics Reports* **145** (1987) 141–249. (Cited on page 2.)

[20] F. Gelis, "A new approach for the vertical part of the contour in thermal field theories," arXiv:hep-ph/9901263 [hep-ph]. (Cited on page 2.)

[21] I. Ojima, "Gauge fields at finite temperatures–"Thermo field dynamics" and the KMS condition and their extension to gauge theories," *Annals of Physics* **137** (1981) 1–32. (Cited on page 2.)

[22] Y. Takahashi and H. Umezawa, "Thermo Field Dynamics," *Collective Phenomena* **2** (1975) 55–80. (Cited on page 2.)

[23] H. Matsumoto, "Vacuum in thermo field dynamics," *Zeitschrift für Physik C Particles and Fields* **34** (1987) 335–339. (Cited on page 2.)

[24] H. Matsumoto, F. Mancini, and M. Marinaro, "Perturbation expansion and initial-state correlations in non-equilibrium thermo-field dynamics," *Journal of Physics A: Mathematical and General* **20** (1987) 6543–6551. (Cited on page 2.)

[25] H. Ahmed, "Nonequilibrium thermofield dynamics," *International Journal of Theoretical Physics* **28** (Nov, 1989) 1351–1357. (Cited on page 2.)

[26] D. Matrasulov, T. Ruzmetov, D. Otajanov, P. Khabibullaev, A. Saidov, and F. Khanna, "Finite-temperature nonlinear dynamics in cavity QED: A thermofield dynamics approach," *Physics Letters A* **373** (2009) 238–242. (Cited on page 2.)

[27] J. Rammer, *Quantum Field Theory of Non-equilibrium States*. Cambridge University Press, Cambridge, 2007. (Cited on pages 2 and 16.)

[28] J. Rammer and H. Smith, "Quantum field-theoretical methods in transport theory of metals," *Rev. Mod. Phys.* **58** (Apr, 1986) 323–359. (Cited on pages 2 and 3.)

[29] M. Cini, "Time-dependent approach to electron transport through junctions: General theory and simple applications," *Phys. Rev. B* **22** (Dec, 1980) 5887–5899. (Cited on page 3.)

[30] M. Cini, *Topics and Methods in Condensed Matter Theory*. Springer-Verlag, Heidelberg, 2007. (Cited on pages 3, 7, and 31.)

[31] Y. Meir and N. S. Wingreen, "Landauer formula for the current through an interacting electron region," *Phys. Rev. Lett.* **68** (Apr, 1992) 2512–2515. (Cited on page 3.)

[32] J. E. Hirsch and R. M. Fye, "Monte Carlo Method for Magnetic Impurities in Metals," *Phys. Rev. Lett.* **56** (Jun, 1986) 2521–2524. (Cited on page 3.)

[33] A. N. Rubtsov, V. V. Savkin, and A. I. Lichtenstein, "Continuous-time quantum Monte Carlo method for fermions," *Phys. Rev. B* **72** (Jul, 2005) 035122. (Cited on pages 3 and 23.)

[34] P. Werner, A. Comanac, L. de' Medici, M. Troyer, and A. J. Millis, "Continuous-Time Solver for Quantum Impurity Models," *Physical Review Letters* **97** (2006) 076405. (Cited on page 3.)

[35] M. Eckstein, M. Kollar, and P. Werner, "Dynamical phase transition in correlated fermionic lattice systems," `arXiv:0904.0976v1 [cond-mat]`. (Cited on pages 3, 46, 52, and 59.)

[36] S. Hofferberth, I. Lesanovsky, B. Fischer, T. Schumm, and J. Schmiedmayer, "Non-equilibrium coherence dynamics in one-dimensional Bose gases," *Nature* **449** (Sep, 2007) 324 – 327. (Cited on pages 3 and 45.)

[37] G. D.Mahan, *Many-particle physics*. Plenum Press, 233 Spring Street, New York, 1986. (Cited on page 7.)

[38] J. W. Negele and H. Orland, *Quantum Many-Particle Systems*. Advanced Book Classics. Westview Press, Boulder, Colorado, 1988. (Cited on pages 13, 14, and 63.)

[39] F. F. Assaad, "Some Notes." 2008. (Cited on page 13.)

[40] D. J. Luitz, "Anwendung der Diagrammatischen Monte-Carlo Methode auf den Josephson - Strom durch einen Quantenpunkt," Master's thesis, Universität Würzburg, Aug, 2008. (Cited on pages 18, 23, and 26.)

[41] A. C. Hewson, *The Kondo Problem to Heavy Fermions*. Cambridge University Press, Cambridge, 1997. (Cited on page 18.)

[42] D. E. Knuth, "Computer Programming as an Art," *Communications of the ACM* **17** (December, 1974) 667–673. (Cited on page 21.)

[43] B. Efron and R.Tibshirani, "Bootstrap Methods for Standard Errors, Confidence Intervals, and Other Measures of Statistical Accuracy," *Statistical Science* **1** (1986) . (Cited on page 22.)

[44] F. F. Assaad and T. C. Lang, "Diagrammatic Determinantal methods: Projective schemes and applications to the Hubbard-Holstein model," *PRB* **76** (2007) , `cond-mat/0702455v2`. (Cited on pages 23, 25, 26, 32, and 38.)

[45] J. Hubbard, "Electron correlations in narrow energy bands," *Proc. R. Soc. London A* **276** (1963) 238. (Cited on page 31.)

[46] F. Gebhard, *The Mott Metal-Insulator Transition*. Springer Verlag, Berlin, 1997. (Cited on page 31.)

[47] G. König and G. Stollhoff, "Why polyacetylene dimerizes: Results of ab initio computations," *Phys. Rev. Lett.* **65** (Sep, 1990) 1239–1242. (Cited on page 31.)

[48] M. Sing, U. Schwingenschlögl, R. Claessen, P. Blaha, J. Carmelo, L. M. Martelo, P. D. Sacramento, M. Dressel, and C. S. Jacobsen, "Electronic structure of the quasi-one-dimensional organic conductor TTF-TCNQ," arXiv:cond-mat/0304283 [cond-mat]. (Cited on page 31.)

[49] G. Stollhof, "Multiband Hubbard Models and the Transition Metals," arXiv:0906.5459v1 [cond-mat]. (Cited on page 32.)

[50] O. Gunnarsson, E. Koch, and R. M. Martin, "Mott transition in degenerate Hubbard models: Application to doped fullerenes," *Phys. Rev. B* **54** (Oct, 1996) R11026–R11029. (Cited on page 32.)

[51] V. J. Emery, "Theory of high-Tc superconductivity in oxides," *Phys. Rev. Lett.* **58** (Jun, 1987) 2794–2797. (Cited on page 32.)

[52] S. Brehm, E. Arrigoni, M. Aichhorn, and W. Hanke, "Theory of two-particle excitations and the magnetic susceptibility in high Tc cuprate superconductors," arXiv:0811.0552v3 [cond-mat]. (Cited on page 32.)

[53] H.-B. Yang, J. Rameau, P. Johnson, T.Valla, A. Tsvelik, and G. D. Gu, "Emergence of preformed Cooper pairs from the doped Mott insulating state in $Bi_2Sr_2CaCu_2O_{8+}$," *Nature* **456** (Nov, 2008) 77–80. (Cited on page 32.)

[54] V. Voroshilov, "On the existence of Cooper pairs in the Hubbard Model," arXiv:0902.1924v1 [cond-mat]. (Cited on page 32.)

[55] I. Bloch, "Quantum Gases," *Science* **319** (Jan, 2008) 1202–1203. (Cited on page 32.)

[56] C. N. Varney, C.-R. Lee, Z. J. Bai, S. Chiesa, M. Jarrell, and R. T. Scalettar, "High Precision Quantum Monte Carlo Study of the 2D Fermion Hubbard Model," arXiv:0903.2519v2 [cond-mat]. (Cited on page 32.)

[57] S. Trotzky, P. Cheinet, S. Fölling, M. Feld, U. Schnorrberger, A. M. Rey, A. Polkovnikov, E. A. Demler, M. D. Lukin, and I. Bloch, "Time-resolved Observation and Control of Superexchange Interactions with Ultracold Atoms in Optical Lattices," *Science* **319** (Jan, 2008) 295–299. (Cited on page 42.)

[58] I. Carusotto, L. Pitaevskii, S. Stringari, G. Modugno, and M. Inguscio, "Sensitive Measurement of Forces at the Micron Scale Using Bloch Oscillations of Ultracold Atoms," *Phys. Rev. Lett.* **95** (Aug, 2005) 093202. (Cited on page 45.)

[59] C. Honerkamp and W. Hofstetter, "Ultracold Fermions and the SU(N) Hubbard Model," *Phys. Rev. Lett.* **92** (Apr, 2004) 170403, arXiv:0309374 [cond-mat]. (Cited on page 45.)

[60] T. Kinoshita, T. Wenger, and D. S. Weiss, "A quantum Newton's cradle," *Nature* **440** (Apr, 2006) 900–903. (Cited on page 45.)

[61] M. Rigol, "Breakdown of Thermalization in Finite One-Dimensional Systems," *Physical Review Letters* **103** (Sep, 2009) , arXiv:0904.3746v2 [cond-mat]. (Cited on pages 45 and 46.)

[62] C. Kollath, A. M. Lauchli, and E. Altman, "Quench Dynamics and Nonequilibrium Phase Diagram of the Bose-Hubbard Model," *Physical Review Letters* **98** (2007) 180601. (Cited on page 45.)

[63] M. Moeckel and S. Kehrein, "Real-time evolution for weak interaction quenches in quantum systems," arXiv:0903.1561 [cond-mat]. (Cited on page 45.)

[64] U. Schneider, L. Hackermuller, S. Will, T. Best, I. Bloch, T. A. Costi, R. W. Helmes, D. Rasch, and A. Rosch, "Metallic and Insulating Phases of Repulsively Interacting Fermions in a 3D Optical Lattice," *Science* **322** (2008) 1520–1525. (Cited on page 46.)

[65] M. Rigol and A. Muramatsu, "Numerical simulations of strongly correlated fermions confined in 1D optical lattices," *Optics Communications* **243** (Dec, 2004) 33–43, arXiv:0412543v1 [cond-mat]. (Cited on page 46.)

[66] M. Rigol, V. Dunjko, V. Yurovsky, and M. Olshanii, "Relaxation in a Completely Integrable Many-Body Quantum System: An Ab Initio Study of the Dynamics of the Highly Excited States of 1D Lattice Hard-Core Bosons," *Physical Review Letters* **98** (2007) 050405. (Cited on page 46.)

[67] E. T. Jaynes, "Information Theory and Statistical Mechanics," *Phys. Rev.* **106** (May, 1957) 620–630. (Cited on page 46.)

[68] E. T. Jaynes, "Information Theory and Statistical Mechanics. II," *Phys. Rev.* **108** (Oct, 1957) 171–190. (Cited on page 46.)

[69] J. M. Deutsch, "Quantum statistical mechanics in a closed system," *Phys. Rev. A* **43** (Feb, 1991) 2046–2049. (Cited on page 46.)

[70] M. Srednicki, "Chaos and quantum thermalization," *Phys. Rev. E* **50** (Aug, 1994) 888–901. (Cited on page 46.)

[71] M. Rigol, V. Dunjko, and M. Olshanii, "Thermalization and its mechanism for generic isolated quantum systems," *Nature* **452** (Apr, 2008) 854–858. (Cited on pages 46 and 47.)

[72] M. Rigol, "Quantum quenches and thermalization in one-dimensional fermionic systems," arXiv:0908.3188v1 [cond-mat]. (Cited on page 46.)

[73] F. F. Assaad, "Some other Notes." 2009. (Cited on pages 47 and 53.)

If I have seen farther than others,
it is because I have stood
on the shoulders of giants.

— Isaac Newton to Robert Hooke

ACKNOWLEDGMENTS

First I am grateful to Prof. Fakher F. Assaad for giving me the possibility to work on this interesting but not very well-known research topic, as well as I thank him for his supervision and assistance during the progress of my thesis.

I'd like to thank David for helping me with:
Physics, QMC, C++, LaTeX, bureaucracy, proofreading this thesis,
and numerous other little things. I also like to thank Burkhard and Jutta for proofreading a lot of this thesis and spotting numerous mistakes. Quite some people contributed to debugging this thesis but nevertheless some will have remained unspotted. The blame for these bugs rests entirely with me. Furthermore I'd like to thank Michi for answering all of my questions and Thomas for providing the workgroup with a coffee-machine. I thank Pete and Peng with whose help I managed to get through the first stages of learning the DDQMC algorithm. I thank the whole TP1 staff for the friendly and fun working atmosphere.

I also like to thank those that studied with me like Christoph, Flo, Max, Michi B., Seb, Patrick and numerous other people that accompanied me through the years of university, and provided the occasional place to sleep.

Special thanks to my computer wthp095 a well as wthp096 that dutifully did their job, leaving out some power outages... I also like to thank every single bit of the 16GB of RAM of wthp104, wthp105 and wthp106 personally that carried most of the workload of the ultracold atom simulations. I also like to thank our admin Guido for keeping those computers running.

I thank my parents for their confidence and encouragement towards achieving this aim, as well as their shuttle-service to the train-station.

Finally I'd like to thank my girlfriend Andrea for her love, hugs, cuddles and moral support as well as sharing me with computers and physics.

Special thanks to caffeine!

DECLARATION

Ich versichere hiermit, dass ich die vorgelegte Diplomarbeit am Institut für Theoretische Physik und Astrophysik der Julius-Maximilians-Universität Würzburg unter der Anleitung von Prof. Dr. Fakher F. Assaad selbstständig durchgeführt und keine anderen Quellen und Hilfsmittel als die angegebenen benutzt habe.

Würzburg, September 2009

Florian Goth